J. Fluid Mech. (2020), *vol.* 885, A30. © The Author(s), 2019.
Published by Cambridge University Press
doi:10.1017/jfm.2019.980

Wall-attached and wall-detached eddies in wall-bounded turbulent flows

Ruifeng Hu[1,2,4], **Xiang I. A. Yang**[3,†] **and Xiaojing Zheng**[4,†]

[1]Key Laboratory of Mechanics on Disaster and Environment in Western China, Ministry of Education, and Department of Mechanics and Engineering Sciences, College of Civil Engineering and Mechanics, Lanzhou University, Lanzhou 731000, China

[2]Department of Mechanical Engineering, Johns Hopkins University, Baltimore, MD 21218, USA

[3]Department of Mechanical Engineering, Pennsylvania State University, State College, PA 16802, USA

[4]Research Center for Applied Mechanics, School of Mechano-Electronic Engineering, Xidian University, Xi'an 710071, China

(Received 3 February 2019; revised 20 September 2019; accepted 19 November 2019)

According to Townsend's attached eddy hypothesis (AEH), a boundary layer flow is comprised of wall-attached eddies, but to extract the part of the flow whose statistical behaviours are well described by the AEH is not at all straightforward. The objective of this work is to extract the part of the flow that can be described by the AEH, and study the statistical behaviours of the other part, which cannot be described by the AEH. In this process, two types of eddies are identified in addition to the Kolmogorov-scale eddies, i.e. wall-attached eddies and wall-detached eddies. The statistical behaviours of the wall-attached eddies are shown to be very well described by the AEH, i.e. the eddies are wall-attached, self-similar and, importantly, Gaussian, whereas the wall-detached eddies cannot be modelled by the AEH. Specifically, a decomposition scheme is proposed following Townsend (*The Structure of Turbulent Shear Flow*, Cambridge University Press, 1976). We apply our decomposition scheme to three different flows, i.e. channel, boundary layer and atmospheric surface layer flows. The results are similar with only quantitative differences, suggesting possible universality in both the wall-attached eddies and the wall-detached eddies.

Key words: boundary layer structure, turbulence theory, turbulent boundary layers

1. Introduction

Coherent structures that span a broad range of length and time scales are common in wall-bounded turbulent flows (Cantwell 1981; Robinson 1991; Adrian 2007; Jiménez 2018). These structures play an important role in generating and sustaining turbulence. Near the wall, turbulence is self-sustaining through a regeneration process independent of the outer motions (Hamilton, Kim & Waleffe 1995; Waleffe 1997; Jiménez & Pinelli 1999; Schoppa & Hussain 2002). In the logarithmic layer and the outer layer, there exist large-scale structures (Adrian 2007; Marusic *et al.* 2010;

† Email addresses for correspondence: xiangyang@psu.edu, xjzheng@xidian.edu.cn

https://doi.org/10.1017/jfm.2019.980 Published online by Cambridge University Press

Smits, McKeon & Marusic 2011; Jiménez 2018), which are further categorized into large-scale motions, hairpin packets (Kovasznay, Kibens & Blackwelder 1970; Brown & Thomas 1977; Adrian, Meinhart & Tomkins 2000; Ganapathisubramani, Longmire & Marusic 2003; Tomkins & Adrian 2003; Deng *et al.* 2018; Wang *et al.* 2019), very-large-scale motions, superstructures (Kim & Adrian 1999; Guala, Hommema & Adrian 2006; Balakumar & Adrian 2007; Hutchins & Marusic 2007; Lee & Sung 2011; Wang & Zheng 2016), etc. These outer motions superimpose on top of and modulate the small-scale inner motions (Rao, Narasimha & Narayanan 1971; Bandyopadhyay & Hussain 1984; Abe, Kawamura & Choi 2004; Hutchins & Marusic 2007; Mathis, Hutchins & Marusic 2009; Chung & McKeon 2010; Ganapathisubramani *et al.* 2012; Dogan *et al.* 2019).

A general objective of turbulence modelling is to understand the statistical behaviours of the coherent motions in the flow. A well-studied phenomenological model is Townsend's attached eddy hypothesis (AEH). The AEH was proposed by Townsend (1976) and has received much attention in the recent literature. According to the AEH, the logarithmic layer may be modelled as an assembly of geometrically self-similar and statistically independent eddies that are attached to the wall. Following the AEH to its logical conclusions, the streamwise and spanwise velocity variances are logarithmic functions of the wall-normal distance y (Townsend 1976), and the wall-normal velocity variance is a constant, i.e.

$$\left.\begin{array}{c} \langle u^{2+}\rangle = B_1 - A_1 \ln(y/\delta), \\ \langle w^{2+}\rangle = B_3 - A_3 \ln(y/\delta), \\ \langle v^{2+}\rangle = B_2, \end{array}\right\} \tag{1.1}$$

where u, v and w are the streamwise, wall-normal and spanwise velocity fluctuations and the superscript $+$ denotes normalization by the friction velocity $u_\tau = \sqrt{\tau_w/\rho}$ and the kinematic viscosity ν. Here τ_w is the wall-shear stress, ρ is the fluid density, δ is the outer length scale, i.e. boundary layer thickness, half-channel height or pipe radius, and A_1, A_3 and $B_{1,2,3}$ are constants. Empirical evidence of (1.1) was not found until quite recently when high-Reynolds-number data became available (Jiménez & Hoyas 2008; Hultmark *et al.* 2012; Marusic *et al.* 2013; Yamamoto & Tsuji 2018). In addition to the scalings in (1.1), several other scalings were identified by studying the AEH. These scalings include the logarithmic law of even-order moments (Meneveau & Marusic 2013), the power law of moment-generating functions (Yang, Marusic & Meneveau 2016*b*), the logarithmic law of two-point correlations (Yang, Marusic & Meneveau 2016*a*; Mouri 2017), the logarithmic law of two-point structure functions (Davidson, Nickels & Krogstad 2006; De Silva *et al.* 2015; Yang *et al.* 2017) as well as the velocity probability distribution scaling (Ge, Yang & Marusic 2019). On the one hand, the presence of these scalings shows the predictive power of the AEH; on the other hand, these scaling can be used to test if the extracted eddies are indeed attached eddies.

Despite the success of the AEH in providing scaling estimates of flow statistics in the logarithmic range, extracting attached eddies, or extracting the part of the velocity field from a flow that is due to attached eddies, is not very straightforward. Depending on the specific criterion to which one resorts, e.g. self-similarity, wall-attachedness, one could get different eddy structures. Del Álamo *et al.* (2006) and Lozano-Durán, Flores & Jiménez (2012) identified three-dimensional vortex clusters and quadrant structures that are geometrically self-similar. Hwang & Sung (2018) extracted structures that lead to a logarithmic scaling of $\langle u^2\rangle$. Hwang (2015) isolated

https://doi.org/10.1017/jfm.2019.980 Published online by Cambridge University Press

wall-attached eddies at a given spanwise length scale. Sharma & McKeon (2013) were able to find wall-attached modes in the framework of resolvent analysis (McKeon & Sharma 2010). Hellström, Marusic & Smits (2016) observed self-similar wall-attached modes from their proper orthogonal decomposition analysis of turbulent pipe flows. Recently, Cheng *et al.* (2019) adopted bidimensional empirical mode decomposition and argued that the third mode corresponds to attached eddies. A shortfall of the above methodologies is that the objective was to identify specific eddies and not to identify a part of the flow whose statistical behaviours are captured by the AEH. In a recent review, Marusic & Monty (2019) pointed out that 'attached eddies are only statistically representative structures and searching for candidate attached eddy shapes from flow visualizations is highly problematic and potentially misleading'. In this work, we will follow Marusic & Monty (2019) and focus on extracting the part of the flow whose statistical properties are captured by the AEH.

While the data support the AEH in general, there are definite inconsistencies between the AEH and the data. First, the logarithmic law of the wall is a good working approximation of the mean flow at moderate Reynolds numbers from about $y^+ = 30$ to about $y/\delta = 0.2$ (Jiménez & Moser 2007; Lee & Moser 2015), but the logarithmic law of the streamwise velocity variance, which should be a good working approximation of $\langle u^2 \rangle$ in the same wall-normal distance range at the same Reynolds-number range as the logarithmic law of the wall, is valid only at high Reynolds numbers and in a comparably much more limited wall-normal distance range (Marusic *et al.* 2013; Yamamoto & Tsuji 2018). Second, according to the AEH, the attached eddies are Gaussian, but the streamwise flow statistics are in reality sub-Gaussian (Meneveau & Marusic 2013; Woodcock & Marusic 2015; Yang *et al.* 2016*b*). Hence it is safe to say that, in addition to attached eddies and small-scale isotropic eddies, there are other types of energy-containing eddies in the flow.

Admitting that the AEH is not a complete description of wall-bounded flows, some studies have attempted to model eddies that are not wall-attached. Perry & Marusic (1995) refined the attached eddy model by incorporating two types of eddies, i.e. type-A and type-B eddies. Type-A eddies are 'wall structures' (wall-attached eddies) and type-B eddies are 'wake structures' (wall-detached eddies). There is also a small amount of turbulence kinetic energy from type-C eddies, which are Kolmogorov-scale eddies (Perry, Henbest & Chong 1986; Perry & Marusic 1995). Recently, Baars & Marusic (2020*a*) proposed a data-based spectral decomposition method. They followed Perry & Marusic (1995) and separated the type-A and type-B eddies using two continuous spectral filters. A log-linear scaling of $\langle u^{2+} \rangle$ with a Townsend–Perry constant of $A_1 = 0.98$ was found, suggesting that type-A eddies might be wall-attached eddies as described in the AEH (Baars & Marusic 2020*b*).

The present study shares a similar objective to that of Baars & Marusic (2020*a*,*b*) and Perry & Marusic (1995), but as will become clear in the later sections, we take a statistical perspective and our discussion is more closely linked to Townsend (1976). We decompose the flow field into 'wall-attached eddies', 'wall-detached eddies' and Kolmogorov-scale eddies. We show that the statistical behaviours of the extracted wall-attached eddies are well described by the AEH. Then, we study the statistical properties of the wall-detached eddies, whose statistical behaviours are not captured by the AEH. Last we study the interaction among the small-scale eddies, the wall-attached eddies and the wall-detached eddies. Recently, Lee & Moser (2019) decomposed the streamwise velocity by applying a spectral filter that cuts off at $\lambda^+ = 1000$, and studied the interaction between the large and the small scales. They found that the large scales project turbulence energy into the near-wall region and control the small scales, which we verify in our work.

https://doi.org/10.1017/jfm.2019.980 Published online by Cambridge University Press

The rest of the paper is organized as follows. Details of the dataset are presented in § 2 along with the decomposition methodology. In § 3, we show that the statistical properties of the extracted part of the flow are captured by the AEH. We study the properties of the detached eddies in § 4, where a phenomenological model for the detached eddies is proposed. Then, we study the interactions between the attached eddies and the detached eddies in § 5. We show the instantaneous flow fields of each type of eddy in § 6, and in § 7 we present our conclusions. Throughout this paper, we use x, y and z to denote the streamwise, wall-normal and spanwise directions, fluctuating velocity components are denoted using lowercase letters, e.g. u is the streamwise velocity fluctuation, and variables in wall units are denoted using superscript $+$.

2. Datasets and methodology

2.1. *Dataset description*

We use three sets of data, i.e. direct numerical simulations of turbulent channel flow (Lee & Moser 2015), hot-wire measurements of zero-pressure-gradient turbulent boundary layers (ZPGTBLs) (Hutchins *et al.* 2009; Philip *et al.* 2013; Baars *et al.* 2015; Marusic *et al.* 2015; Baidya 2016) and field measurements of an atmospheric surface layer (ASL) (Wang & Zheng 2016).

The direct numerical simulations solve the incompressible Navier–Stokes equations in a periodic channel (Lee, Malaya & Moser 2013). The computation domain is $8\pi \times 2 \times 3\pi$ in the streamwise (x), wall-normal (y) and spanwise (z) directions, respectively. The half-channel height is unity. The friction Reynolds numbers of the direct numerical simulations are $Re_\tau \approx 1000$, 2000 and 5200. The dataset is maintained by the University of Texas at Austin, and the data at $Re_\tau \approx 1000$ and 5200 can be accessed through the Johns Hopkins Turbulence Database (http://turbulence.pha.jhu.edu/) (Graham *et al.* 2016).

The ZPGTBL data are hot-wire measurements in the High Reynolds Number Boundary Layer Wind Tunnel at the University of Melbourne (Hutchins *et al.* 2009; Marusic *et al.* 2015). The wind tunnel has a test section of 27 m. The Reynolds numbers are from $Re_\tau \approx 2800$ to 13 000. We also adopt data of two-point synchronous hot-wire measurement at $Re_\tau \approx 15\,000$ (Baars *et al.* 2015; Baars, Hutchins & Marusic 2017) and the x-wire measurements of ZPGTBL flow at $Re_\tau \approx 10\,000$ (Philip *et al.* 2013; Baidya 2016). The sampling rate is 20 kHz and the non-dimensional sampling interval is $\Delta T^+ \approx 1.3$. The measurement lasted for about $TU_\infty/\delta = 20\,000$.

The ASL data are field measurements at the Qingtu Lake Observation Array (QLOA) site in western China under near-neutral atmospheric stratification conditions (Wang & Zheng 2016). The Reynolds number is as high as $Re_\tau \sim O(10^6)$. Sonic anemometers (Gill Instruments R3-50 and Campbell CSAT3B) were installed to record the three velocity components at a sampling rate of 50 Hz. The raw data are split into multiple one-hour segments for subsequent analysis, and the non-dimensional time duration of each segment is $TU_\infty/\delta = 200$–400, during which the flow is roughly statistically stationary.

2.2. *A decomposition scheme*

Following the discussion in the introduction, it is known that not all the eddies are wall-attached. In this section, we propose a decomposition scheme that extracts the velocity induced by wall-attached eddies. The scheme follows directly from

https://doi.org/10.1017/jfm.2019.980 Published online by Cambridge University Press

Townsend (1976). The objective is to extract the part of the velocity field that is due to wall-attached eddies (rather than to extract specific eddies that are wall-attached). According to Townsend (1976): first, sizes of wall-attached eddies scale as their distances from the wall; second, the streamwise and the spanwise velocities at a distance from the wall are a superposition of eddy-induced velocities; third, at a distance from the wall, the wall-normal velocity component is solely due to the attached eddy at that distance because of the wall blocking effect. These three statements are discussed in further detail in, for example, Perry & Chong (1982), Meneveau & Marusic (2013) and Yang & Meneveau (2019). It follows from the three statements that attached eddies are responsible for the streamwise and spanwise velocities of scale

$$\alpha_{1,3} y < \lambda_x < \beta_{1,3}\delta, \quad \gamma_{1,3} < y^+, \tag{2.1a,b}$$

where α, β and γ are constants, and the subscripts 1 and 3 denote the streamwise and the spanwise velocity components. Because attached eddies are not isotropic flow structures, α_1, β_1 and γ_1 are not necessarily equal to α_3, β_3 and γ_3. The constant γ is a viscous cutoff, the lower limit αy scales with y because attached eddies scale with their distances from the wall and the upper limit scales with δ because the largest eddies, which scale with δ, also contribute to the streamwise velocity at y. For the wall-normal velocity component, the attached eddies are responsible for the scales

$$\alpha_2 y < \lambda_x < \beta_2 y, \quad \gamma_2 < y^+. \tag{2.2a,b}$$

The upper limit scales with y instead of δ because the larger scales do not contribute to the local wall-normal velocity.

The velocities of scales in (2.1) and (2.2) are due to wall-attached eddies. This means that a subset of these scales are also induced by wall-attached eddies. A direct implication is that, if a set of constants, i.e. $\alpha_{1,2,3}$, $\beta_{1,2,3}$ and $\gamma_{1,2,3}$, are appropriate for extracting attached eddy-induced flow fields, any $\alpha'_{1,2,3}$, $\beta'_{1,2,3}$ and $\gamma'_{1,2,3}$ such that

$$\gamma'_{1,2,3} > \gamma_{1,2,3}, \quad \alpha'_{1,2,3} > \alpha_{1,2,3}, \quad \beta'_{1,2,3} < \beta_{1,2,3} \tag{2.3a–c}$$

will also be appropriate for extracting attached eddy-induced flow fields. It is only if we use $\alpha'_{1,2,3}$, $\beta'_{1,2,3}$ and $\gamma'_{1,2,3}$ instead of $\alpha_{1,2,3}$, $\beta_{1,2,3}$ and $\gamma_{1,2,3}$ that some scales that could have been included as attached eddies would be precluded.

2.3. *The pre-multiplied velocity spectra of wall-attached eddies*

Following the discussion in the previous section, although we could be conservative in choosing the constants, the idea is to find $\alpha_{1,2,3}$, $\beta_{1,2,3}$ and $\gamma_{1,2,3}$ such that as many scales as possible are included in (2.1) and (2.2). Because our scheme in § 2.2 is a scale decomposition one, it is most natural to start our discussion from the velocity spectra. The spectrum of a single wall-attached eddy is the topic of, for example, Baidya *et al.* (2017). Nonetheless, not too much is known about the spectrum of an assembly of wall-attached eddies. In the following, we will derive the velocity spectra due to an assembly of wall-attached eddies.

In figure 1(*a*), we sketch three hierarchies of attached eddies. Here, the inclination angle is ϕ. The geometric representation in figure 1(*a*) is not meant to be taken literally. In general, $\tan\phi = l_y/l_x \approx y/l_x$ and $l_x \approx y/\tan\phi$, where l_y is the eddy height and l_x is the streamwise extent of the eddy. Note that y/l_x could also be regarded as the wall/normal-streamwise aspect ratio of attached eddies. The corresponding

https://doi.org/10.1017/jfm.2019.980 Published online by Cambridge University Press

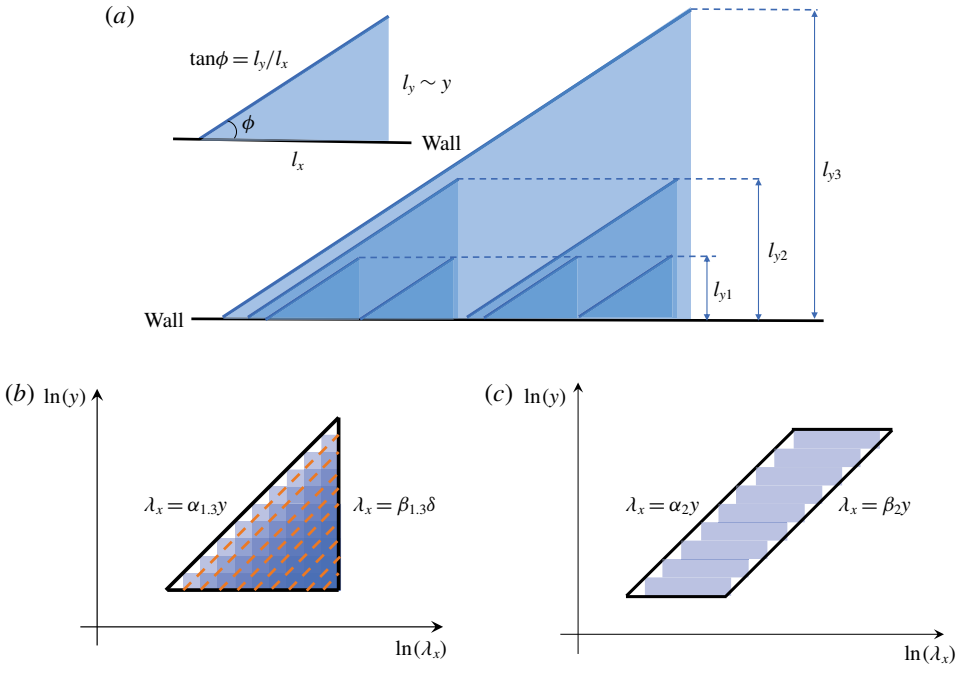


FIGURE 1. (*a*) Sketch of three hierarchies of wall-attached eddies. A typical attached eddy is also sketched. (*b*) The resulting pre-multiplied spectrum of the streamwise/ spanwise velocity due to nine hierarchies of attached eddies. (*c*) The resulting pre-multiplied spectrum of the wall-normal velocity due to nine hierarchies of attached eddies.

pre-multiplied streamwise (spanwise) velocity energy spectrum $k_x E_{uu}$ ($k_x E_{ww}$) is sketched in figure 1(*b*), where k_x is the streamwise wavenumber and E_{uu} (E_{ww}) is the streamwise (spanwise) energy spectrum. In the following, our discussion will focus on the streamwise velocity component with the understanding that a similar argument applies to the spanwise velocity component. Eddies of height y contribute to the pre-multiplied spectrum in $\alpha_1 y < \lambda_x < \beta_1\delta$, $\gamma_1 < y^+$ and $y < l_y$, where $\beta_1\delta$ and $\alpha_1 y$ are the largest and the smallest streamwise (spanwise) velocity length scale at height $l_y = y$, and $\gamma_1 \approx 100$ is the viscous cutoff (Perry & Chong 1982). Adding contributions from all wall-attached eddies, the attached eddies are responsible for the region enclosed by the triangle in figure 1(*b*), in which region the scaling of the contour levels is $\lambda_x \sim y$. Baars, Hutchins & Marusic (2017) carried out a similar analysis for the spectral coherence spectrum. In the context of this work, it is more straightforward to do this analysis for the pre-multiplied energy spectra, the integration of which leads to the kinetic energy. Next, let us derive the pre-multiplied wall-normal velocity spectrum. This is comparably simpler because the local wall-normal velocity is solely controlled by the local wall-attached eddies (Townsend 1976; Perry & Chong 1982; Yang *et al.* 2018). Figure 1(*c*) shows the pre-multiplied wall-normal velocity spectrum, where there is no superposition of contributions from eddies of different sizes.

https://doi.org/10.1017/jfm.2019.980 Published online by Cambridge University Press

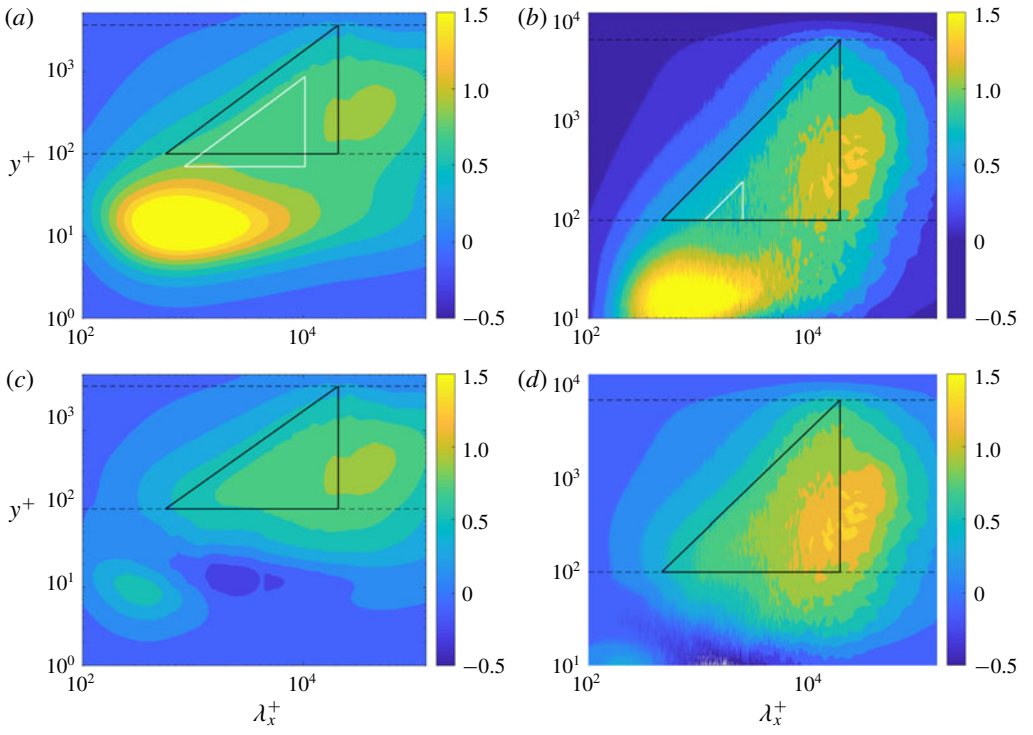


FIGURE 2. Pre-multiplied streamwise velocity spectra in (*a*) a $Re_\tau = 5200$ channel and (*b*) a $Re_\tau = 13\,000$ ZPGTBL, and spectra with the inner scales removed in (*c*) a $Re_\tau = 5200$ channel and (*d*) a $Re_\tau = 13\,000$ ZPGTBL. The thin dashed lines are at the viscous cutoff $y^+ = 100$ and the height of the largest attached eddies. The white triangle in (*a*) corresponds to (2.5) and that in (*b*) corresponds to (2.4). The black triangles are the present decomposition scheme.

2.4. *The velocity spectrum*

There is no guarantee that the spectral behaviour derived above could be found in reality. In this subsection, we take a look at the measured pre-multiplied velocity spectra, and see if figure 1 is consistent with the data. We show $k_x E_{uu}^+$ in a $Re_\tau = 5200$ channel and a $Re_\tau = 13\,000$ ZPGTBL in figures 2(*a*) and 2(*b*), respectively. Removing the inner-scale motions according to Hu & Zheng (2018), the remaining parts of the spectra are shown in figure 2(*c*,*d*). The regions enclosed in the black triangles exhibit the predicted behaviour, and, according to our discussion in the previous subsection, these regions represent velocities due to wall-attached eddies.

An extensively studied scaling is the k_x^{-1} law of the streamwise velocity spectrum (Perry & Chong 1982; Perry *et al.* 1986), based on which one could also claim a region in the velocity spectrum that represents contributions from wall-attached eddies. These regions are similar to ours in that they enclose a triangular region of the velocity spectrum, although these studies did not make a connection between this triangular region and the behaviour of $\langle u^2 \rangle$. For instance, Nickels *et al.* (2005) proposed the following region for boundary layers:

$$y^+ > 100, \quad \lambda_x \geqslant 15.7y \quad \text{and} \quad \lambda_x \leqslant 0.3\delta, \tag{2.4a–c}$$

https://doi.org/10.1017/jfm.2019.980 Published online by Cambridge University Press

and Hwang (2015) proposed

$$y^+ > 70, \quad \lambda_x \geqslant 12y \quad \text{and} \quad \lambda_x \leqslant 2\delta \tag{2.5a–c}$$

for a channel, both of which are shown in figure 2. Depending on the flow quantity at which one looks, the definition of the logarithmic layer, or the scales that are relevant to the logarithmic layer, could be very different. For example, if one looks at the mean flow, one may claim that the logarithmic layer is from $y^+ = 30$ to $y/\delta = 0.2$, but if one looks at the streamwise velocity variance, one may argue that the logarithmic layer is from $y^+ = 3\sqrt{Re_\tau}$ to $y/\delta = 0.15$ (Marusic *et al.* 2013). Compared to the scalings we look at in this work, i.e. the $y \sim \lambda_x$ scaling of the pre-multiplied velocity spectrum, the k^{-1} scaling is much more difficult to find (Mouri, Morinaga & Haginoya 2019). Hence, although Hwang (2015), Nickels *et al.* (2005) and we are looking for the parts of the velocity spectrum that represent contributions from wall-attached eddies, the claimed regions in Hwang (2015) and Nickels *et al.* (2005) and by us will be different.

The remaining parts of the streamwise velocity spectrum, i.e. the parts outside the triangle, are not due to wall-attached eddies. The small-scale eddies, i.e. $\lambda_x < \alpha_1 y$, are roughly isotropic. Their contributions to the turbulent kinetic energy are usually small at high Reynolds numbers. The larger-scale motions, i.e. $\lambda_x > \beta_1 \delta$ in the pre-multiplied spectrum, contribute significantly to the turbulent kinetic energy. For reasons that will be clear in a later section, we will refer to the motions that are responsible for the region $\lambda_x > \beta_1 \delta$ in the pre-multiplied spectrum as 'detached eddies'.

We make a note about the connections and the differences between the present definitions and those in the literature. The type-A eddies in Perry & Marusic (1995) are attached eddies. The type-B and type-C eddies are similar to the detached eddies and the small-scale eddies defined herein. The 'detached eddies' in Perry & Marusic (1995), Katul & Vidakovic (1996), Jiménez (2012) and Agostini & Leschziner (2017) are Kolmogorov-scale eddies similar to our small-scale eddies.

Having looked at the streamwise velocity spectrum, we take a look at the spanwise and the wall-normal velocity spectra. The pre-multiplied spanwise and wall-normal velocity spectra are shown in figures 3(*a*) and 3(*b*), respectively, in a $Re_\tau \approx 10\,000$ ZPGTBL. The predicted behaviours are found in the triangular region (2.1) and parallelogram region (2.2).

2.5. *Constants in the decomposition*

To extract the wall-attached motions, we need to determine the constants in (2.1) and (2.2). Following the discussion in § 2.2, we could be conservative and leave out some of the attached eddies, but here we hope to include all the scales that represent contributions from attached eddies. Per figure 2, $\alpha_1 = 5.7$ and $\gamma_1 = 100$. The viscous cutoff is $\gamma_1 = 100$ as follows from Perry & Chong (1982). The small-scale cutoff follows from the inclination angle of streamwise velocity signals, i.e. $\alpha_1 = 1/\tan(\phi_1)$, where $\phi_1 \approx 10^\circ$ is the inclination angle of streamwise velocity signals (Brown & Thomas 1977; Adrian *et al.* 2000; Christensen & Adrian 2001; Marusic & Heuer 2007; De Silva, Hutchins & Marusic 2016; Liu, Bo & Liang 2017). The large-scale cutoff is $\beta_1 = 3$ for boundary layer and $\beta_1 = 4$ for channel, considering that the large scales in channel are longer than those in boundary layer (Monty *et al.* 2009). If the same, more conservative constant $\beta_1 = 3$ is used for both channel and boundary layer, the extracted part of the flow would still be due to wall-attached eddies, but we will miss scales that should have been included in the context of channel flow. Per figure 3, $\gamma_{2,3} = 100$, $\alpha_{2,3} = 1$, $\beta_3 = 1$ and $\beta_2 = 5$. The viscous cutoff for the

https://doi.org/10.1017/jfm.2019.980 Published online by Cambridge University Press

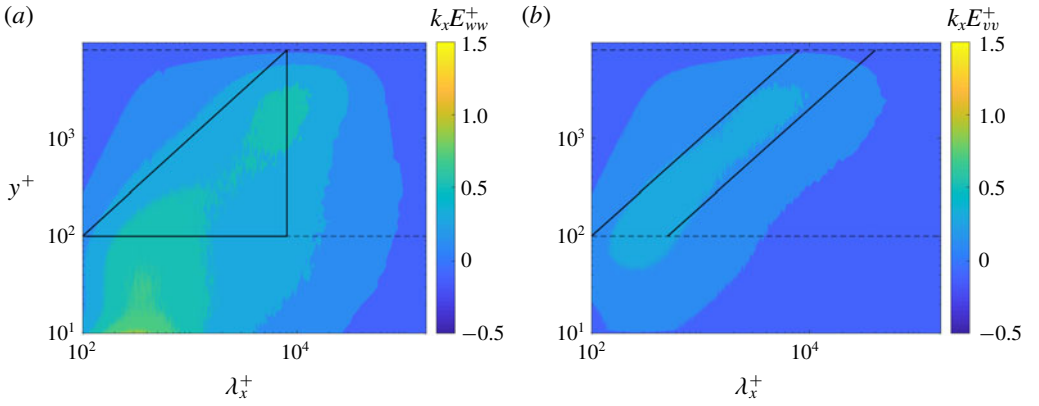


FIGURE 3. Pre-multiplied spectra of the transverse velocity components in ZPGTBL flow at $Re_\tau \approx 10\,000$: (*a*) the spanwise velocity; (*b*) the wall-normal velocity.

spanwise and the wall-normal velocity is the same as that for the streamwise velocity. The longitudinal scales of the spanwise and wall-normal velocity components are smaller than the streamwise component (Del Álamo *et al.* 2004; Jiménez & Hoyas 2008; Hwang 2015; Hwang & Sung 2018; Yang & Bo 2018; Cheng *et al.* 2019), and hence $\alpha_{2,3} < \alpha_1$. The specific value $\alpha_{2,3} = 1$ corresponds to a 45° inclination angle of spanwise and wall-normal velocity signals (Head & Bandyopadhyay 1981). According to our discussion in 2.2, the AEH should provide a complete statistical description of the scales in these regions.

3. Wall-attached eddies

In § 2.4, we showed that the AEH is able to predict the behaviour of the pre-multiplied velocity spectrum in the enclosed regions in figures 2 and 3. If the AEH is valid, by applying the spectral decomposition (2.1) to the datasets in § 2.1, we should be able to extract the part of the flow whose statistical properties (including the behaviour of the velocity spectrum but also the behaviour of other statistical flow quantities) are captured by the AEH. In this section, we will carefully test if this is true by comparing statistical properties of the extracted eddies to the predictions of the AEH. We will be able to conclude that the AEH is a good model for the extracted part of the flow if the statistical properties of the extracted scales are captured by the AEH. In the following, we focus on the streamwise velocity component and also show results for the spanwise and the wall-normal velocity components.

3.1. *Velocity variances*

The logarithmic variation of the streamwise velocity variance is probably the most well-known consequence of the AEH (Townsend 1976):

$$\left\langle (u^+_{AE})^2 \right\rangle = D_1 - C_1 \ln(y/\delta). \tag{3.1}$$

We can rewrite the above equation (3.1) as

$$\left\langle (u^+_{AE})^2 \right\rangle = C_1 \ln(\delta_i/y), \quad \delta_i = (\beta_1/\alpha_1)\delta, \tag{3.2a.b}$$

https://doi.org/10.1017/jfm.2019.980 Published online by Cambridge University Press

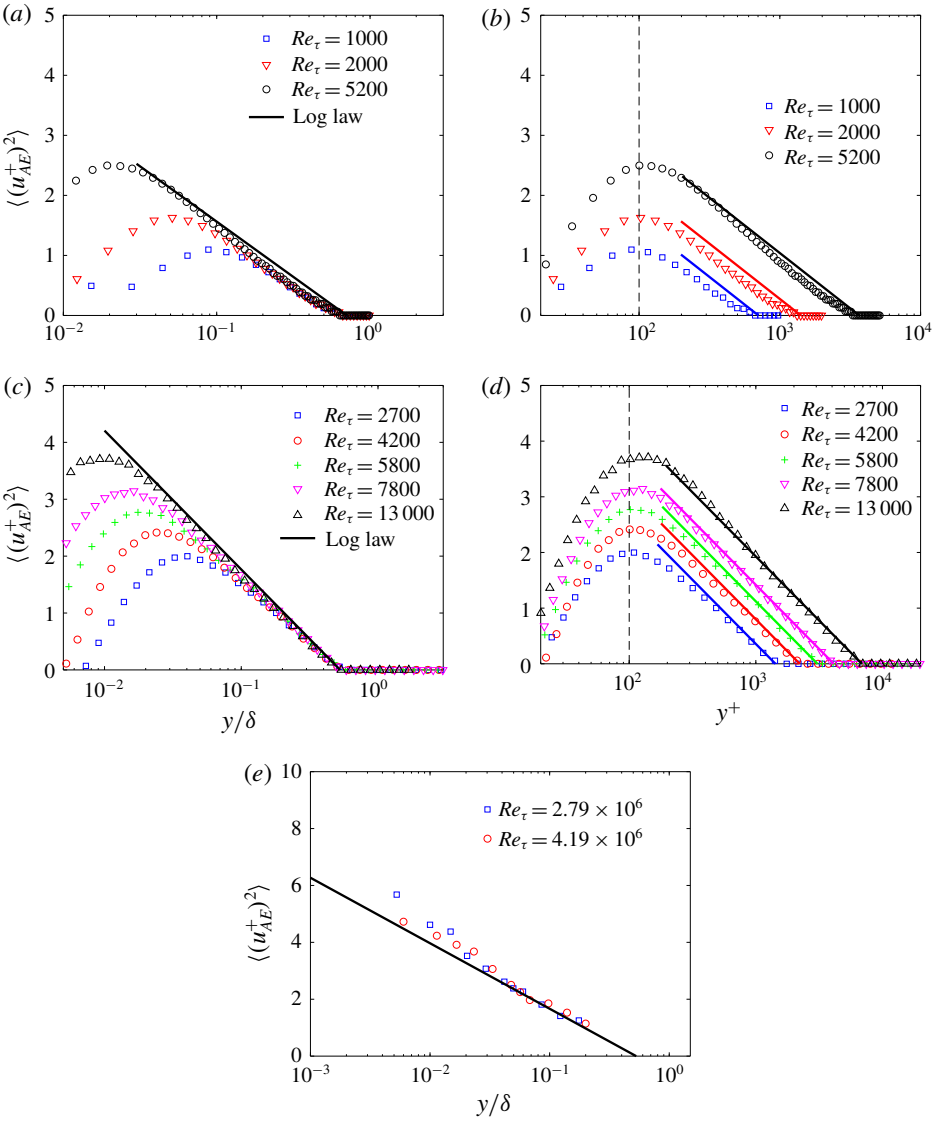


FIGURE 4. Streamwise velocity variances of the attached eddies in turbulent channel flow (*a*,*b*), ZPGTBL flow (*c*,*d*) and ASL flow (*e*). The solid lines correspond to (3.2*a*.*b*), with $C_1 = 0.8$ for turbulent channel flows, and $C_1 = 1.0$ for ZPGTBL flows and ASL flows.

where $\langle (u^+_{AE})^2 \rangle = 0$ at $y = \delta_i$. In previous literature, although the logarithmic scaling of the streamwise velocity variance was found, its wall-normal extent and the Reynolds number range of the scaling found are not entirely consistent with the AEH. Figure 4 shows the streamwise velocity variance of the attached eddies in turbulent channel flow, ZPGTBL and ASL. The Reynolds number spans about three decades, i.e. Re_τ from $O(10^3)$ to $O(10^6)$. The logarithmic scaling of $\langle (u^+_{AE})^2 \rangle$ starts at $y^+ \sim O(10^2)$, i.e. the viscous cutoff, and ends at $y = \delta_i$, following precisely the prediction of the AEH. The constant C_1 is 0.8 in channel flow and 1.0 in boundary layer flow. The measurement of Baars & Marusic (2020*b*) shows that $C_1 = 0.98$ in boundary layer,

https://doi.org/10.1017/jfm.2019.980 Published online by Cambridge University Press

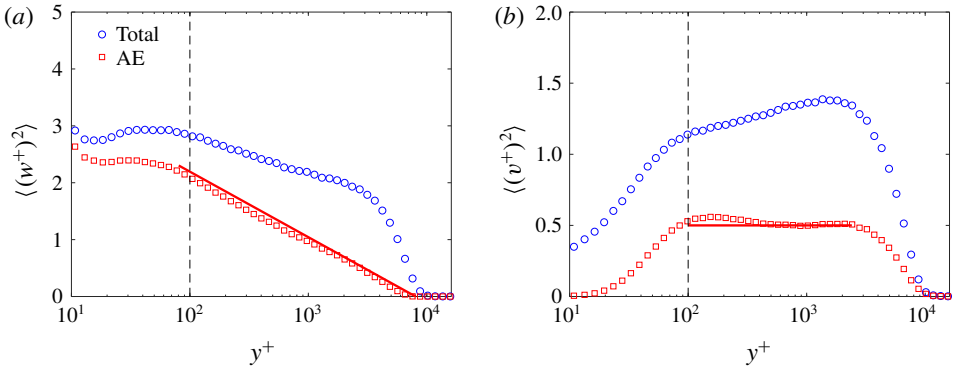


FIGURE 5. Variances of transverse velocity components in ZPGTBL flow at $Re_\tau \approx 10\,000$: (*a*) spanwise velocity; (*b*) wall-normal velocity. The solid lines correspond to (3.3), with $C_3 = 0.5$ and $D_2 = 0.5$. AE, attached eddies.

which is very close to our measurement here. It is noted that the scaling of streamwise velocity variance was also considered by other approaches (Monkewitz & Nagib 2015; Vassilicos *et al.* 2015; Laval *et al.* 2017; Chen, Hussain & She 2018).

Figure 5 shows the spanwise and wall-normal velocity variances due to the attached eddies in a $Re_\tau = 10\,000$ boundary layer. According to the AEH,

$$\left\langle (w^+_{AE})^2 \right\rangle = D_3 - C_3 \ln(y/\delta), \quad \left\langle (v^+_{AE})^2 \right\rangle = D_2, \tag{3.3a,b}$$

which are consistent with the data in figure 5.

Several recent studies reported similar results. Ganapathisubramani (2018) applied a high-pass frequency filter $f^+ = 0.005$ to ZPGTBL measurement data and found a universal logarithmic law of the small-scale streamwise velocity variance. Lee & Moser (2019) applied a high-pass spectral filter $\lambda^+ = 1000$ to turbulent channel flow data (Lee & Moser 2015), and found a logarithmic scaling of the small-scale streamwise and spanwise velocity fluctuations. Nonetheless, because the extracted part of the flow in those two studies does not exactly correspond to the triangular region in figure 1(*b*), in principle, one could not claim that the observed scalings in those two studies are results of attached eddies, and because those two studies did not compare other statistical properties of the extracted eddies to the predictions of the AEH, one probably could not claim with confidence that the extracted eddies are the attached eddies as described in the AEH.

In order to claim that the extracted eddies are wall-attached eddies, every aspect of the statistical properties of the extracted eddies should be captured by the AEH. Next, we will take a look at other statistics.

3.2. *High-even-order moments*

Meneveau & Marusic (2013) concluded from the AEH that high-even-order moments behave logarithmically as a function of the wall-normal distance:

$$\langle (u^+)^{2p} \rangle^{1/p} = B_{1,p} - A_{1,p} \ln(y/\delta), \tag{3.4}$$

where $A_{1,p} = A_1[(2p-1)!!]^{1/p}$ because of the presumed Gaussianality of the wall-attached eddies, $n!! \equiv n(n-2)(n-4)\ldots 1$ is the double factorial and A_1 is the

https://doi.org/10.1017/jfm.2019.980 Published online by Cambridge University Press

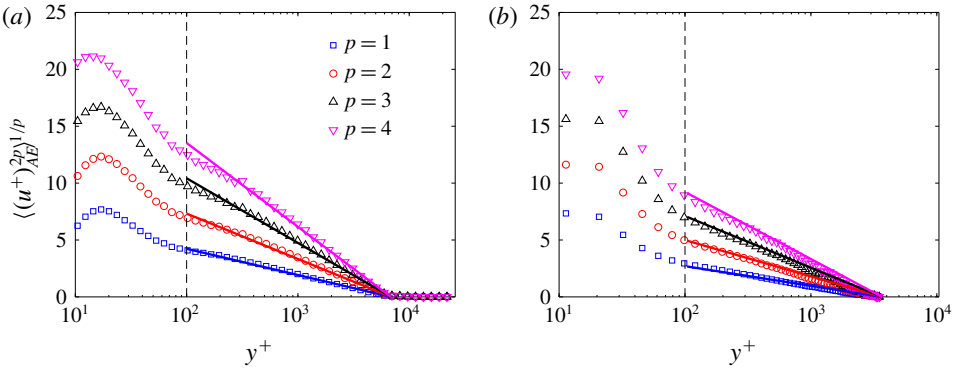


FIGURE 6. High-even-order central moments of streamwise velocity due to the attached eddies in (*a*) turbulent boundary layer flow at $Re_\tau = 13\,000$ and (*b*) turbulent channel flow at $Re_\tau = 5200$. The solid lines correspond to (3.5). The slopes of the solid lines correspond to $C_{1,p} = C_1[(2p-1)!!]^{1/p}$ with $C_1 = 1.0$ (ZPGTBL) or 0.8 (channel), and are not best fits to the data.

Townsend–Perry constant (Marusic *et al.* 2013). They argued that because the velocity increment due to each wall-attached eddy is identical and independent, the summation of these velocity increments is Gaussian as per the central limit theorem. This follows directly from Townsend, where he argued that all attached eddies are independent and the flow field is 'homogeneous' in terms of the appearance of wall-attached eddies. While the logarithmic scaling was found, the measured slopes A_p are sub-Gaussian instead of Gaussian.

Following Meneveau & Marusic (2013), for attached eddies, the even-order moments should follow

$$\langle (u^+_{AE})^{2p} \rangle^{1/p} = C_{1,p} \ln(\delta_i/y), \tag{3.5}$$

$$\langle (w^+_{AE})^{2p} \rangle^{1/p} = C_{3,p} \ln(\delta_i/y), \tag{3.6}$$

where $C_{1,p} = C_1[(2p-1)!!]^{1/p}$ and $C_{3,p} = C_3[(2p-1)!!]^{1/p}$. We test if that is the case. We can claim success only if (i) the predicted scaling is found and (ii) the pre-factors are Gaussian.

Figure 6 shows the high-even-order moments of streamwise velocity of the attached eddies for $p = 1, 2, 3, 4$ in a ZPGTBL flow at $Re_\tau = 13\,000$ and turbulent channel flow at $Re_\tau = 5200$, and figure 7 shows those of the spanwise velocity in a ZPGTBL flow at $Re_\tau = 10\,000$. The data are compared to (3.5) and (3.6), and reasonably good agreements are found. Note that, as far as the attached eddies are concerned, the data are very much Gaussian.

3.3. *Moment-generating functions*

Invoking the AEH, Yang *et al.* (2016*b*) concluded that the moment-generating functions (MGFs), i.e. $\langle \exp(qu^+) \rangle$ (q is an arbitrary real number), follow a power-law scaling as follows:

$$W(q; y) = \langle \exp(qu^+) \rangle = \left(\frac{y}{\delta_i} \right)^{-\tau(q)}, \tag{3.7}$$

https://doi.org/10.1017/jfm.2019.980 Published online by Cambridge University Press

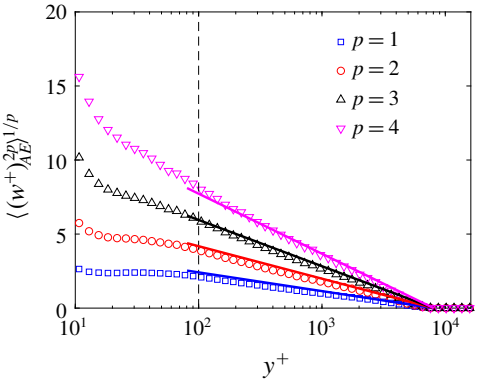


FIGURE 7. High-even-order central moments of spanwise velocity due to the attached eddies in ZPGTBL flow at $Re_\tau \approx 10\,000$. The solid lines correspond to $C_{3,p} = C_3[(2p-1)!!]^{1/p}$ with $C_3 = 0.5$, and are not best fits to the data.

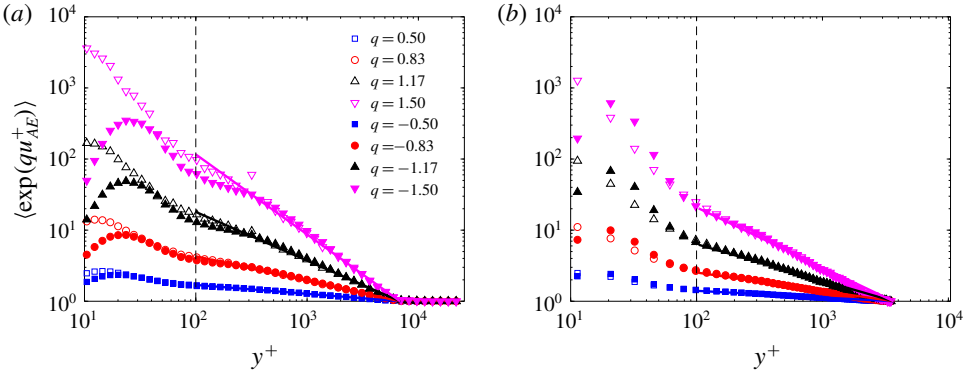


FIGURE 8. Streamwise MGFs of streamwise velocity by the attached eddies in (*a*) turbulent boundary layer flow at $Re_\tau = 13\,000$ and (*b*) turbulent channel flow at $Re_\tau = 5200$. The solid lines correspond to (3.7) and are not fits to the data.

where δ_i is the height of the largest wall-attached eddy in the flow. The scaling exponent $\tau(q)$ is given by

$$\tau(q) = \sigma q^2. \tag{3.8}$$

If the attached eddies are Gaussian, the constant $\sigma = C_1/2$. Similar to Meneveau & Marusic (2013), the data do not support the assumed Gaussianality, and deviations from (3.8) at large and particularly negative q were reported. Here, we compare the MGFs of the extracted attached eddies to the above two scaling predictions. Again, we can claim success only if the predicted power-law scalings are found and if the data are Gaussian.

Figure 8 shows the MGFs of the attached eddies in ZPGTBL flow at $Re_\tau = 13\,000$ and turbulent channel flow at $Re_\tau = 5200$ for $q = -1.5$ to 1.5. Power-law scalings are found. The MGFs with $\pm q$ collapse in the logarithmic layer ($y^+ > 100$) and the predicted symmetry in (3.7) is borne out. In figure 9, we compare the measured $\tau(q)$ to (3.8). The data are Gaussian.

https://doi.org/10.1017/jfm.2019.980 Published online by Cambridge University Press

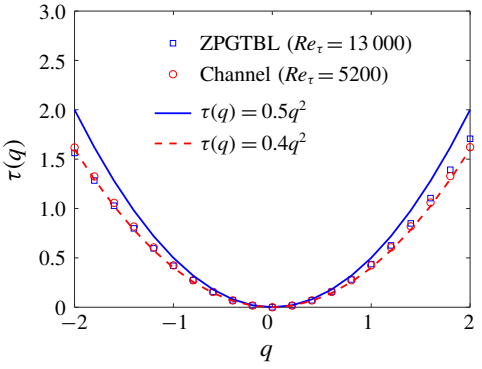


FIGURE 9. The power-law exponent $\tau(q)$ of the MGF in ZPGTBL flow at $Re_\tau = 13\,000$ and channel flow at $Re_\tau = 5200$. The solid lines correspond to (3.8).

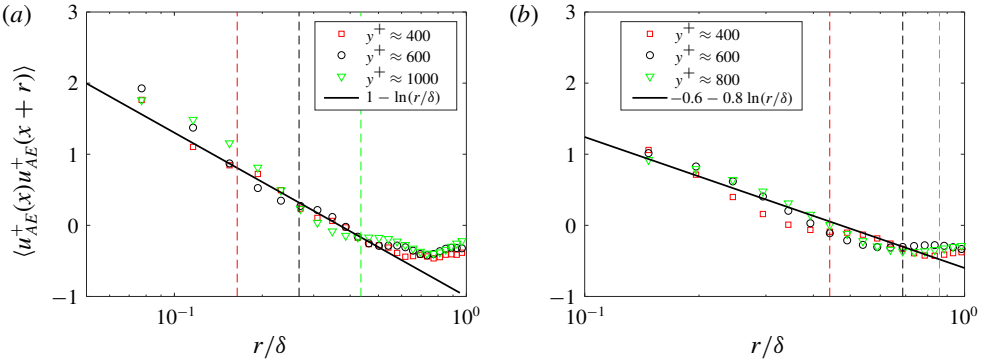


FIGURE 10. The streamwise correlation functions of streamwise velocity by the attached eddies in (*a*) ZPGTBL flow at $Re_\tau = 13\,000$ and (*b*) turbulent channel flow at $Re_\tau = 5200$. The dashed lines correspond to the upper limits ($r_{max} = y/\tan\phi$) of the logarithmic scaling of the two-point correlation function at different heights.

3.4. *Two-point correlation and structure function*

Last, we examine two-point statistics. According to the AEH, the two-point velocity correlation scales as (Yang *et al.* 2016*a*)

$$\langle u^+(x)u^+(x+r)\rangle = B_1' - C_1\ln(\delta/r), \tag{3.9}$$

where B_1' is a constant and C_1 is the same constant in (3.2*a*,*b*). If the AEH is valid, the above scaling is valid for $r \lesssim y/\tan\phi$. Figure 10 shows the streamwise velocity correlation due to the attached eddies in ZPGTBL flow at $Re_\tau = 13\,000$ and turbulent channel flow at $Re_\tau = 5200$. The logarithmic scaling in (3.9) is found with the predicted slope in the expected two-point displacement range.

The same exercise could be done for the structure function, which scales as (Davidson *et al.* 2006; Chung *et al.* 2015; De Silva *et al.* 2015; Yang *et al.* 2017)

$$\langle(\Delta u^+)^2\rangle = 2C_1\ln(r/y) + E_1, \tag{3.10}$$

where E_1 is a constant. Figure 11 shows the structure function in both ZPGTBL and channel flows. Equation (3.10) provides a good working approximation of the statistics in the expected range of two-point displacement.

https://doi.org/10.1017/jfm.2019.980 Published online by Cambridge University Press

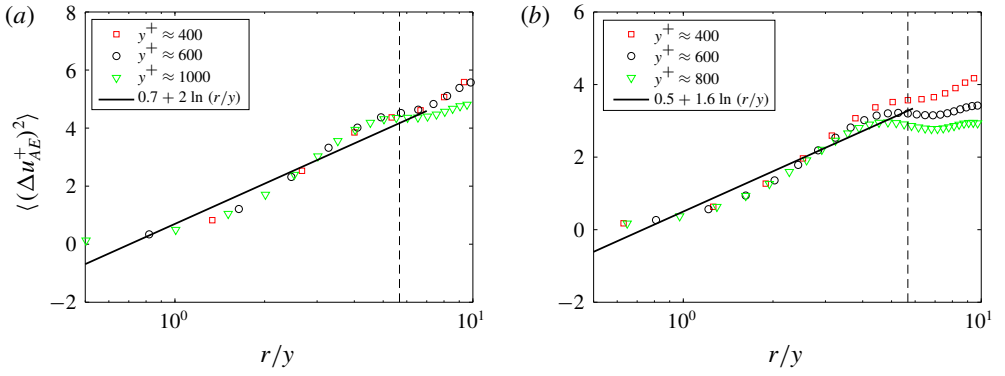


FIGURE 11. The streamwise structure functions of the attached eddies in (*a*) ZPGTBL flow at $Re_\tau = 13\,000$ and (*b*) turbulent channel flow at $Re_\tau = 5200$. The dashed line corresponds to the upper limit ($r_{max}/y = 1/\tan\phi$) of the logarithmic scaling of the two-point structure function at different heights.

3.5. *Summary of wall-attached eddies*

In summary, we have extracted attached eddies according to the AEH, and the various statistical properties (one-point moments and MGFs, two-point correlation and structure function) of the extracted attached eddies are compared to the predictions of the AEH. Fairly good agreements are found in terms of the scaling, the constants in the scaling and the wall-normal extents of the scalings. Most notably, the extracted part of the flow is Gaussian. Hence, we may conclude that the extracted part of the flow is truly due to wall-attached eddies as described in the AEH, i.e. the eddies are wall-attached, self-similar and Gaussian.

4. Wall-detached eddies

In the previous section, we showed that the AEH is a good model for the extracted part of the flow (according to (2.1) and (2.2)). In this section, we turn our attention to the part of the flow that cannot be modelled by the AEH. Unlike the attached eddies, whose statistical behaviours are well described by the AEH, the detached eddies lack a good phenomenological model. Here, we start by examining the statistical properties of the detached eddies and see if we can get a few insights into their organization.

4.1. *Streamwise velocity variance*

Figure 12 shows the streamwise velocity variances of detached eddies in turbulent channel flow, ZPGTBL flow and ASL flow. Unlike $\langle (u^+_{AE})^2 \rangle$, which peaks at the wall ($y^+ \sim O(10^2)$), the streamwise turbulence intensity of the detached eddies $\langle (u^+_{DE})^2 \rangle$ peaks at the centre of the logarithmic layer. This suggests that the detached eddies centre at a distance away from the wall, which is why we had referred to these eddies as detached eddies.

For the boundary layer data, it appears that $\langle (u^+_{DE})^2 \rangle$ follows approximately logarithmic scalings both to the left and to the right of the peak location of $\langle (u^+_{DE})^2 \rangle$. To diagnose the two scalings, we subtract the logarithmic part of the scaling from $\langle (u^+_{DE})^2 \rangle$. The compensated plots are shown in the insets of figure 12(*c*,*d*), and we see plateaus. We could also compare the quality of these logarithmic scalings to

https://doi.org/10.1017/jfm.2019.980 Published online by Cambridge University Press

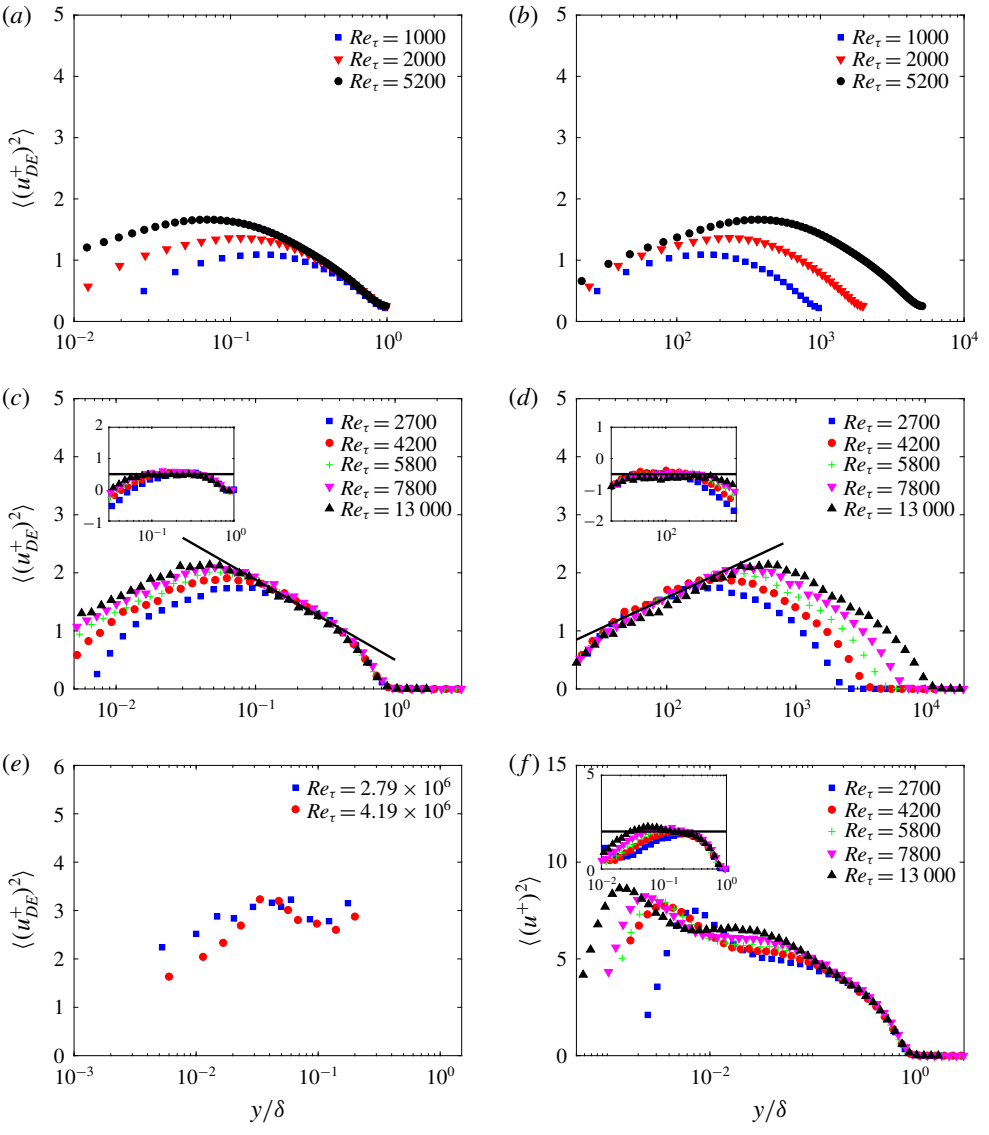


FIGURE 12. Streamwise velocity variances of the detached eddies in turbulent channel flow (*a*,*b*), ZPGTBL flow (*c*,*d*) and ASL flow (*e*). (*f*) The total streamwise velocity variances in ZPGTBL flows. The insets in (*c*) and (*d*) plot $\langle (u^+_{DE})^2 \rangle + 0.6 \log(y/\delta)$ and $\langle (u^+_{DE})^2 \rangle - 0.45 \log(y^+)$ as a function of y/δ and y^+, respectively. The inset in (*f*) plots $\langle (u^+)^2 \rangle + 1.25 \log(y/\delta)$.

the well-accepted logarithmic law of the total streamwise velocity $\langle (u^+)^2 \rangle$ in the ZPGTBL flow data. Comparing figures 12(*c*), 12(*d*) and 12(*f*), it should be clear that the quality of the logarithmic scalings in figure 12(*f*) are equally good (or equally bad) as the ones in figure 12(*c*,*d*). Compared to the boundary layer data, the channel flow data are at a moderate Reynolds number and the ASL data are subjected to freestream/thermal effects. Consequently, only hints of these two logarithmic scalings could be found in channel and ASL data.

https://doi.org/10.1017/jfm.2019.980 Published online by Cambridge University Press

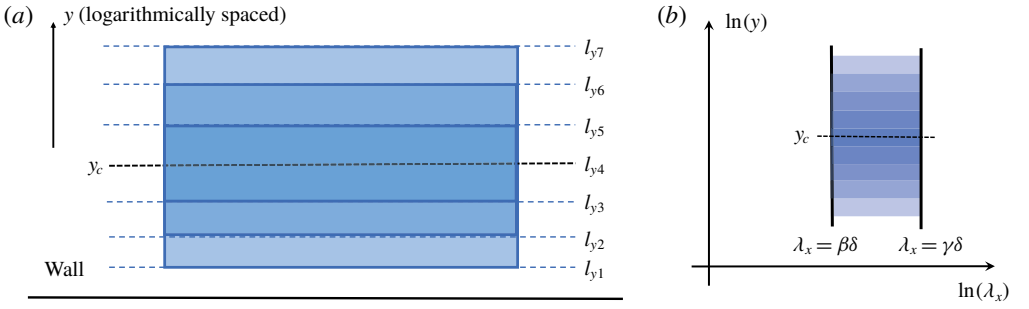


FIGURE 13. Sketches of (*a*) three hierarchies of wall-detached eddies; $l_{yn} = 2^{n-1} l_{y1}$. (*b*) The resulting pre-multiplied spectrum of the streamwise velocity fluctuations due to five hierarchies of detached eddies.

If we follow Townsend, the two logarithmic scalings in $\langle u_{DE}^2 \rangle$ imply that the detached eddies may be modelled as a series of eddies centred at y_c, as sketched in figure 13. If the detached eddies do organize as in figure 13, determining the centre location y_c is probably the most important. In the absence of viscous effects, the centre location y_c corresponds to the peak location of $\langle (u_{DE}^+)^2 \rangle$. Figure 14 shows the wall-normal positions and the magnitudes of $\max[\langle (u_{DE}^+)^2 \rangle]$. The Reynolds number dependence of $y_{DE,max}$ is unclear from the available data. The results of turbulent channel and ZPGTBL flows seem to suggest that $y_{DE,max}^+ = 3.9\sqrt{Re_\tau}$ between $Re_\tau \sim O(10^3)$ and $O(10^4)$, but the ASL data seem to suggest that $(y/\delta)_{DE,max} \to 0.045$. Last, from figure 14(*c*), we see that the peak value $\langle (u_{DE}^+)^2 \rangle_{max}$ follows a logarithmic scaling with respect to the Reynolds number, which is consistent with previous studies (Pullin, Inoue & Saito 2013; Vincenti *et al.* 2013; Vallikivi, Hultmark & Smits 2015).

In Lee & Moser (2019), the authors defined the large scales as $\lambda^+ > 1000$. The streamwise velocity variance due to such defined large scales has a peak. The peak value $\langle (u^+)^2 \rangle_{LS}$ increases and the peak location y/δ decreases as a function of the Reynolds number. In figure 14(*b*), the location is shown for comparison. The difference is probably expected considering the difference in our definitions.

4.2. *High-even-order moments and MGFs*

If the organization of the detached eddies is as sketched in figure 13, following the same argument that leads to the logarithmic scaling of the even-order moments, we expect logarithmic scaling of the even-order moments for the detached eddies to the left and to the right of y_c. Figure 15 shows the even-order moments and MGFs of the detached eddies. Hints of possible logarithmic scalings as a function of the wall-normal distance are found in Figure 15(*a*) to the left and to the right of y_c, as well as hints of possible power-law scalings of the MGFs, but because of the limited extents of the scale ranges to the left and to the right of $y_{c,DE}$, neither of the two scalings is very conclusive.

5. Inter-scale interactions

Having looked at the statistical properties of the attached eddies and the detached eddies separately, in this section we study the interactions between the small-scale eddies, the attached eddies and the detached eddies. Here, we focus on the particular

https://doi.org/10.1017/jfm.2019.980 Published online by Cambridge University Press

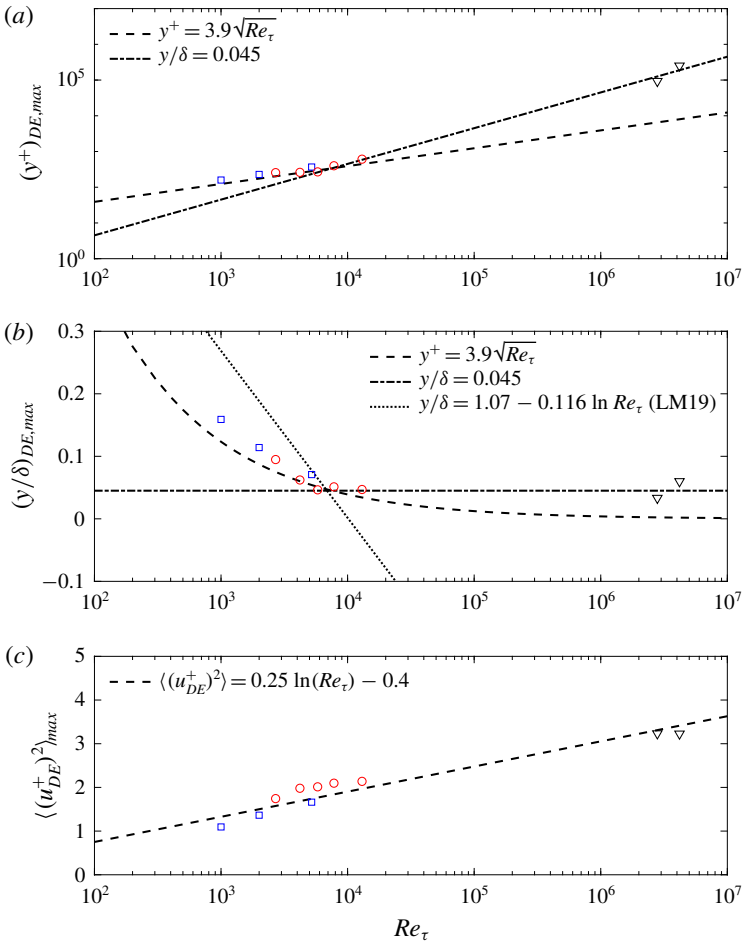


FIGURE 14. The wall-normal locations (*a*,*b*) and the magnitudes (*c*) of the maximum streamwise turbulence intensity due to the detached eddies as a function of the Reynolds number. The squares are turbulent channel flow data. The red circles are boundary layer data. The black triangles are ASL data. The Reynolds number variance of the peak location y/δ with $\lambda^+ > 1000$ from Lee & Moser (2019) is indicated by LM19 in (*b*).

inter-scale interaction of amplitude modulation, where the (loosely defined) small-scale eddies are modulated by the (loosely defined) large-scale eddies. This form of inter-scale interaction has received considerable attention in the recent literature (Hutchins & Marusic 2007; Mathis *et al.* 2009; Chung & McKeon 2010; Guala, Metzger & McKeon 2011; Ganapathisubramani *et al.* 2012; Agostini & Leschziner 2014; Anderson 2016; Dogan, Hanson & Ganapathisubramani 2016; Pathikonda & Christensen 2017, 2019; Howland & Yang 2018; Liu, Wang & Zheng 2019).

In anticipation of the results, we briefly review one of the previously used quantifications of amplitude modulation in Mathis *et al.* (2009):

$$R = \frac{\langle u_L^+ E_L(u_S^+) \rangle}{\mathrm{STD}(u_L^+)\mathrm{STD}(E_L(u_S^+))}, \tag{5.1}$$

https://doi.org/10.1017/jfm.2019.980 Published online by Cambridge University Press

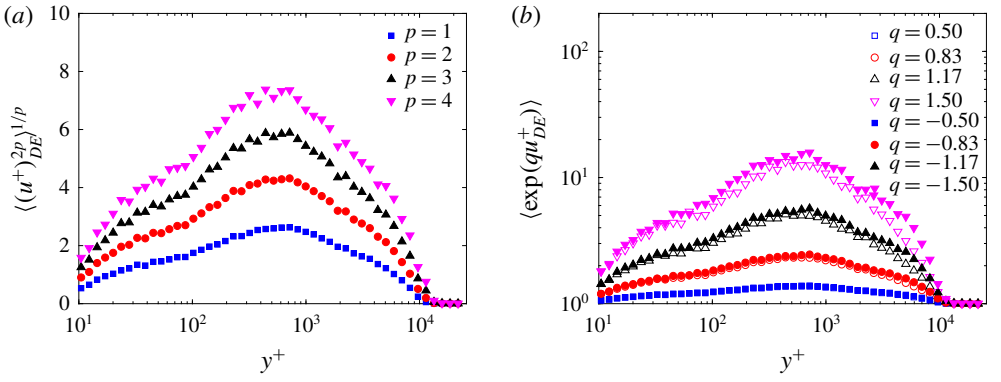


FIGURE 15. Even-order moments (*a*) and MGFs (*b*) of streamwise velocity by the detached eddies in turbulent boundary layer flows at $Re_\tau = 13\,000$.

where u_S and u_L are the (loosely defined) small- and large-scale components of the streamwise velocity, $E(\cdot)$ is the envelope of the bracketed signal and STD$(\cdot)$ is the standard deviation of the bracketed quantity. Thus-defined R behaves similarly to the skewness factor $S = \langle (u^+)^3 \rangle / \langle (u^+)^2 \rangle^{3/2}$ (Schlatter & Örlü 2010). Mathis *et al.* (2011) compared R and S and showed that the behaviour of $\langle 3u_L^+ u_S^{+2} \rangle / \langle (u^+)^2 \rangle^{3/2}$ is similar to that of R, which may serve as an alternative measure of amplitude modulation. Recently, Duvvuri & McKeon (2015) showed that $\langle 3u_L^+ u_S^{+2} \rangle / \langle (u^+)^2 \rangle^{3/2}$ is proportional to R for any statistically stationary signal. Following the previous literature, in the following, we will use the scale-decomposed skewness to quantify amplitude modulation.

In this work, we have decomposed the streamwise velocity fluctuation into SE (small-scale eddies), AE (attached eddies) and DE (detached eddies), and therefore the skewness factor can be decomposed triadically, i.e.

$$\begin{aligned}\langle (u^+)^3 \rangle &= \langle (u^+_{SE} + u^+_{AE} + u^+_{DE})^3 \rangle \\ &= \langle (u^+_{SE})^3 \rangle + \langle (u^+_{AE})^3 \rangle + \langle (u^+_{DE})^3 \rangle + 3\langle (u^+_{SE})^2 u^+_{AE} \rangle + 3\langle (u^+_{AE})^2 u^+_{SE} \rangle \\ &\quad + 3\langle (u^+_{SE})^2 u^+_{DE} \rangle + 3\langle (u^+_{DE})^2 u^+_{SE} \rangle \\ &\quad + 3\langle (u^+_{AE})^2 u^+_{DE} \rangle + 3\langle (u^+_{DE})^2 u^+_{AE} \rangle \\ &\quad + 6\langle u^+_{SE} u^+_{AE} u^+_{DE} \rangle. \end{aligned} \tag{5.2}$$

In figure 16, we show the wall-normal dependence of a few dominant components in (5.2) in the ZPGTBL flow at $Re_\tau = 13\,000$ and the channel flow at $Re_\tau = 5200$. The skewness of the attached eddies, i.e. S_2 in figure 16, is very close to zero in both the ZPGTBL and channel flows. This is consistent with the assumed Gaussian behaviour of the attached-eddy-induced velocities in the AEH. The most significant contributions to S come from the detached eddies, the small-scale eddies and their interactions. The interaction between the attached eddies and the detached eddies, i.e. $3\langle (u^+_{SE})^2 u^+_{AE} \rangle$, is very close to zero and is not shown in figure 16. The results suggest that, at a given wall-normal location, the main inter-scale interaction is among the detached eddies and the small-scale eddies. A recent study using the QLOA dataset also reported a similar one-point multi-scale amplitude-modulation phenomenon (Liu *et al.* 2019).

The above analysis is one-point analysis. Next, we study the modulation of the near-wall turbulence by the attached eddies and the detached eddies. To do that, we use the

https://doi.org/10.1017/jfm.2019.980 Published online by Cambridge University Press

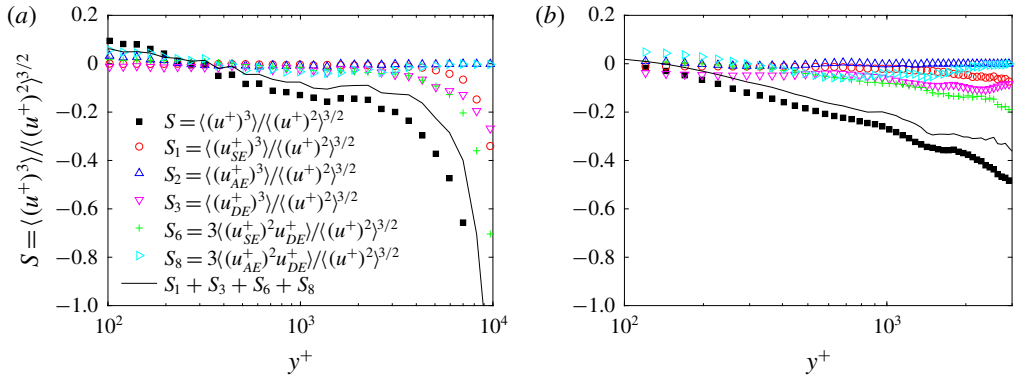


FIGURE 16. Skewness of the streamwise velocity in (*a*) ZPGTBL flow at $Re_\tau = 13\,000$ and (*b*) turbulent channel flow at $Re_\tau = 5200$. ■, $S = \langle (u^+)^3 \rangle / \langle (u^+)^2 \rangle^{3/2}$; ○, $S_1 = \langle (u^+_{SE})^3 \rangle / \langle (u^+)^2 \rangle^{3/2}$; △, $S_2 = \langle (u^+_{AE})^3 \rangle / \langle (u^+)^2 \rangle^{3/2}$; ▽, $S_3 = \langle (u^+_{DE})^3 \rangle / \langle (u^+)^2 \rangle^{3/2}$; +, $S_6 = 3\langle (u^+_{SE})^2 u^+_{DE} \rangle / \langle (u^+)^2 \rangle^{3/2}$; ▷, $S_8 = 3\langle (u^+_{AE})^2 u^+_{DE} \rangle / \langle (u^+)^2 \rangle^{3/2}$; black solid line, $S_1 + S_3 + S_6 + S_8$.

two-point synchronous measurements in ZPGTBL flow at $Re_\tau = 15\,000$ (Baars *et al.* 2015) and turbulent channel flow data at $Re_\tau = 5200$ (one snapshot). We measure the amplitude modulation of the near-wall turbulence by the outer flow using the following correlation coefficient defined in Bernardini & Pirozzoli (2011):

$$C_{AM}(y_1, y_2) = \langle u_L(y_1) E_L(u_S(y_2)) \rangle \tag{5.3}$$

in which y_1 and y_2 are the wall-normal locations of the traversing and fixed probes, respectively ($y_2^+ = 4.33$ is fixed), u_L may be the attached eddies, the detached eddies or the large-scale modes with $\lambda_x^+ > 7000$ and $u_S(y_2)$ is the near-wall small-scale signal with $\lambda_x^+ < 7000$, following Mathis, Hutchins & Marusic (2011). We apply a time shift at y_1 in (5.3) to account for the inclination of the turbulent eddies. Note that, because the attached eddies are not formally defined at a wall-normal distance smaller than the viscous cutoff, i.e. $y^+ = 100$, the near-wall small-scale turbulence, defined as $\lambda_x^+ < 7000$, does not formally overlap with the attached eddies.

Figure 17 shows the wall-normal variations of $C_{AM}(y_1)$ with different $u_L(y_1)$ in ZPGTBL flow. We see that the coefficient calculated with the large-scale modes of $\lambda_x^+ > 7000$ has a peak at $y^+ = 300$–400. The coefficients calculated with the attached or detached eddies are reminiscent of their one-point intensities: the amplitude modulation by the detached eddies has its peak at the centre of the logarithmic region, while that by the attached eddies decreases log-linearly with the wall-normal height. Similar results are obtained in turbulent channel flow at $Re_\tau = 5200$, which are presented in a two-dimensional $C_{AM}(y_1, y_2)$ map in figure 18. The present results suggest that both the attached and detached eddies contribute to the amplitude modulation of the near-wall small-scale motions. Nonetheless, their contributions are quantitatively different.

6. Instantaneous features of the decomposed eddies

Townsend only defined attached eddies in a statistical sense, without attaching any specific geometry to the attached eddies, nor relating any instantaneous flow features

https://doi.org/10.1017/jfm.2019.980 Published online by Cambridge University Press

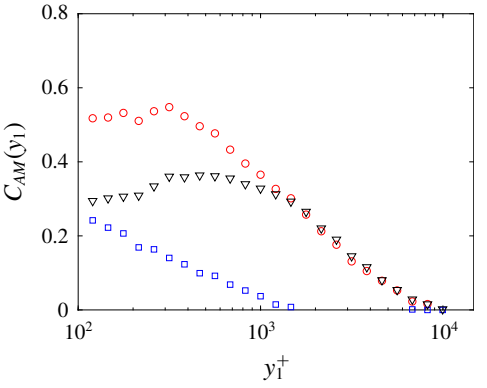


FIGURE 17. Two-point amplitude-modulation coefficient $C_{AM}(y_1)$ in ZPGTBL flow at $Re_\tau = 15\,000$, where u_L is the the large-scale modes of $\lambda_x^+ > 7000$ (○), the attached eddies (□) or the detached eddies (▽).

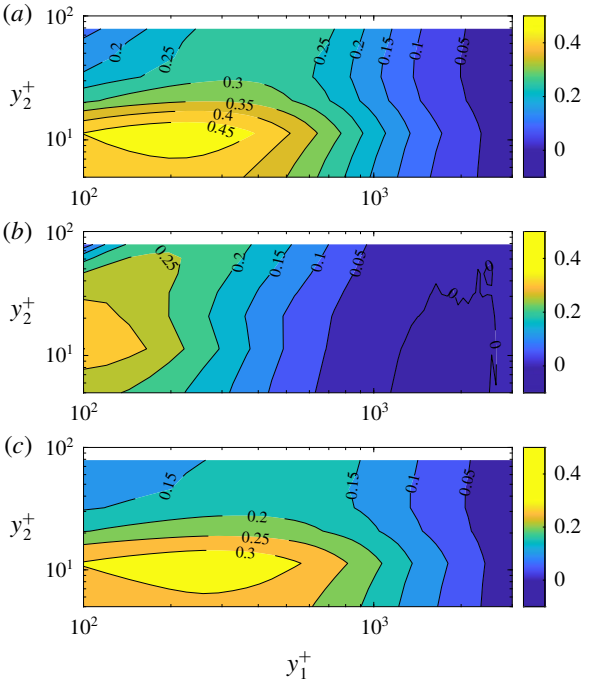


FIGURE 18. Two-point amplitude-modulation coefficient map $C_{AM}(y_1, y_2)$ in turbulent channel flow at $Re_\tau = 5200$ computed with the velocity signals from the (*a*) large-scale modes ($\lambda_x^+ > 7000$), (*b*) attached eddies and (*c*) detached eddies.

to the attached eddies. So far, we have followed Townsend and have focused on the statistical behaviour of the decomposed eddies. Nonetheless, taking a look at the instantaneous velocity fields that correspond to the decomposed eddies would still be instructive. Figure 19 shows the $|u^+| = 1$ isosurfaces of the total velocity, the small-scale eddies, the attached eddies and the detached eddies in channel flow at

https://doi.org/10.1017/jfm.2019.980 Published online by Cambridge University Press

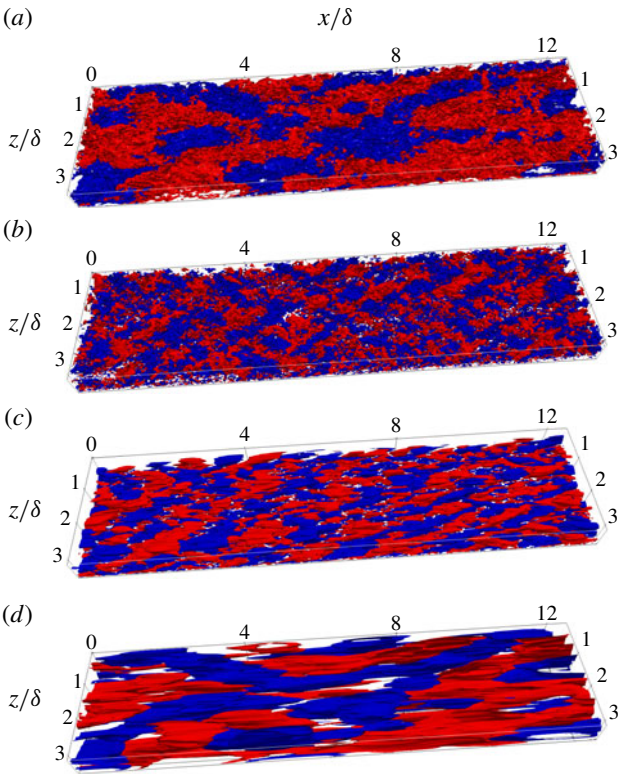


FIGURE 19. Instantaneous $|u^+| = 1$ isosurfaces (red for positive and blue for negative values) from the (*a*) total eddies, (*b*) small-scale eddies, (*c*) attached eddies and (*d*) detached eddies.

$Re_\tau = 5200$. For better presentation, the figure shows the instantaneous velocities in a truncated domain of $0 \leqslant x \leqslant 4\pi$, $100 \leqslant y^+$, $y \leqslant \delta_i$ and $0 \leqslant z \leqslant \pi$. We see alternating high- and low-speed regions in every component. Meandering streaks are found in the velocity field due to detached eddies. Both the attached eddies and the small scales show coherence in oblique orientations with respect to the streamwise direction. Considering that attached eddies (and detached eddies) are only defined from a statistical standpoint, we will refrain from discussing details of the instantaneous flow fields.

7. Conclusions

According to Townsend, the attached eddies in the AEH are defined only in a statistical sense, being responsible for part of the scales in the flow field. Following Townsend (1976), we proposed a scale decomposition scheme and extracted the part of the flow that is due to attached eddies from boundary layer, channel and atmospheric boundary layer flows. By comparing the statistical properties of the extracted eddies to those promised by the AEH, we showed that the AEH is a good model for the extracted part of the flow, and notably that part of the flow is Gaussian. Hence, the reason that the AEH does not capture some of the statistical behaviours of the flow in the logarithmic layer is because there are other energy-containing

https://doi.org/10.1017/jfm.2019.980 Published online by Cambridge University Press

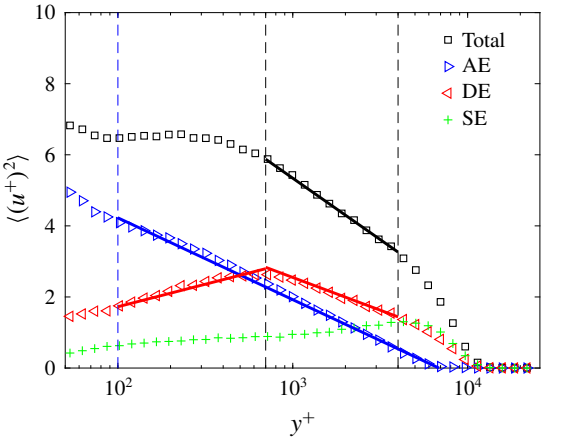


FIGURE 20. Streamwise velocity variance with decomposition of specific contributions by the attached eddies (AE), the detached eddies (DE) and the small-scale eddies (SE).

eddies than the attached eddies, which are the small (Kolmogorov)-scale eddies and the large-scale detached eddies. Unlike the attached eddies whose statistical behaviours are well captured by the AEH, the detached eddies lack a well-validated phenomenological model. In this work, we studied the statistical properties of the detached eddies. Although not conclusive, the statistical behaviour of the detached eddies suggests that these eddies can be modelled as flow structures centred at the midpoint of the logarithmic layer. Finally, we studied the interaction among the small-scale eddies, the attached eddies and the detached eddies. We focused on the particular inter-scale interaction of amplitude modulation. We found first that at a given wall-normal height, the main inter-scale interaction is between the small-scale eddies and the detached eddies, and second that both the attached and detached eddies contribute to the amplitude modulation of the near-wall small-scale motions. Putting together the AEH and our phenomenological model for the detached eddies, we can phenomenologically explain the appearance of the streamwise turbulence kinetic energy plateau in the mesolayer, i.e. $100 < y^+ < 700$, in ZPGTBL flow at $Re_\tau = 13\,000$ as shown in figure 20. In this region, the streamwise turbulence kinetic energy of the attached eddies decreases as a function of y but that of the detached eddies increases as a function of y. The overall effect is the plateau in the total streamwise turbulence kinetic energy. Last, an interesting but unexplored question is whether we could apply a spanwise filter to extract wall-attached eddies. One difficulty in so doing is the determination of the spanwise extent of wall-attached eddies. While Jiménez & Hoyas (2008), Hwang (2015), Hellström *et al.* (2016) and Hwang & Sung (2018) looked at the spanwise scale of attached eddies, compared to the streamwise extent, the spanwise extent of the attached eddies is still less well established.

Acknowledgements

We express our sincere gratitude to I. Marusic, N. Hutchins, W. J. Baars and R. Baidya for providing the Melbourne wind-tunnel measurement data, G.-H. Wang and H.-H. Gu for providing the QLOA data, M. Lee and R. Moser for making the channel flow database publicly available, Z. Wu for aiding in the access of the channel

https://doi.org/10.1017/jfm.2019.980 Published online by Cambridge University Press

flow data in the Johns Hopkins Turbulence Database, as well as C. Meneveau and D. Gayme for helpful suggestions. The authors also appreciate the valuable comments made by the anonymous referees which help to improve both the quality and the presentation of this paper. Financial support by grants from the National Natural Science Foundation of China (11490553, 11972175) is gratefully acknowledged. R.H. is grateful for the hospitality of the Department of Mechanical Engineering of the Johns Hopkins University and the financial support of the China Scholarship Council for his visit.

Declaration of interests

The authors report no conflict of interest.

Appendix A. The effect of filter

Considering (2.1) and (2.2), a sharp cutoff filter is used to extract the part of the flow that is due to wall-attached eddies. In this appendix, we show that the type of filter does not affect much, if at all, our results. Here, we use a continuous spectral filter comparing the results with those from using a sharp filter. The continuous spectral filter is defined based on a hyperbolic tangent function as

$$f_{AE}(\lambda_x, y; A) = H(\lambda_x, y; A) \cdot G(\lambda; A), \tag{A 1}$$

in which $H(\lambda_x, y; A)$ and $G(\lambda, \delta; A)$ correspond to the small-scale and large-scale cutoffs in (2.1), where

$$H(\lambda_x, y; A) = \frac{1 + \tanh\left[A \cdot \ln(\lambda_x/(\alpha y))\right]}{2}, \tag{A 2}$$

$$G(\lambda, \delta; A) = \frac{1 + \tanh\left[A \cdot \ln(\lambda_x/(\beta \delta))\right]}{2} \tag{A 3}$$

and A is the parameter controlling the sharpness of the filter. In the logarithmic layer, the local wall-normal coordinate provides a local length scale (and in the absence of the viscous effects, that is the only length scale). Hence, the sharpness scales with y at the small-scale cutoff and δ at the large-scale cutoff.

Figure 21(*a*) shows the filters with various A values. The sharpness at the small- and large-scale cutoffs increases as A increases. The filter with $A = 5$ is rather smooth, whereas that with $A = 100$ is very close to the sharp cutoff filter in (2.1) and (2.2). We apply the continuous filter with various A values to the ZPGTBL flow data at $Re_\tau = 13\,000$, and the resulting streamwise velocity variances of the attached eddies are shown in figure 21(*b*). The results are essentially the same, indicating that the sharpness of the filter will probably not affect our conclusions.

Appendix B. The effect of large-scale cutoff wavelength

In § 2.2, we argued that using a more conservative cutoff, the extracted part of the flow will still be fully described by the AEH. Here, we show that this statement is true. In addition, we show that an aggressive cutoff will include scales that do not belong to attached eddies and have a negative impact on the results. We choose two different large-scale cutoffs, namely $\lambda_x = \delta$ ($\beta_1 = 1$) and $\lambda_x = 10\delta$ ($\beta_1 = 10$). In the main text, $\lambda_x = 3\delta$ ($\beta_1 = 3$) for ZPGTBL flow. Figure 22(*a*) shows the enclosed regions. The

https://doi.org/10.1017/jfm.2019.980 Published online by Cambridge University Press

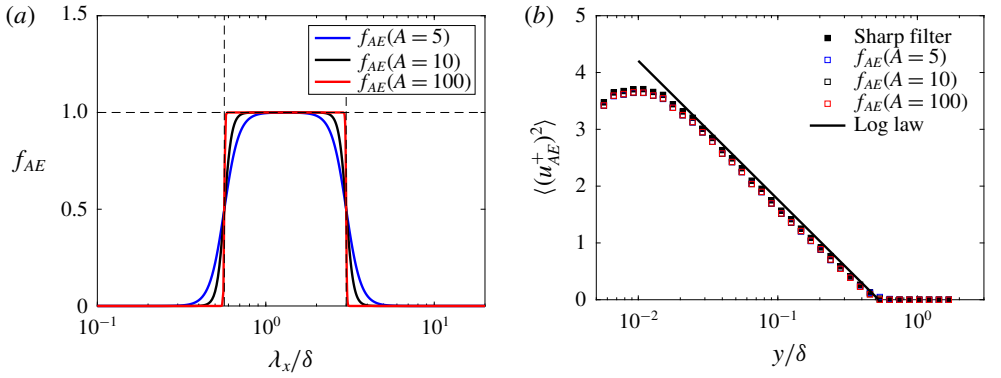


FIGURE 21. The effect filter on the statistics of attached eddies. (*a*) Continuous filters with different values of A. The wall-normal location is $y/\delta = 0.1$. (*b*) The streamwise velocity variances obtained with different filters in (*a*). The solid line corresponds to the logarithmic law (3.2*a*.*b*).

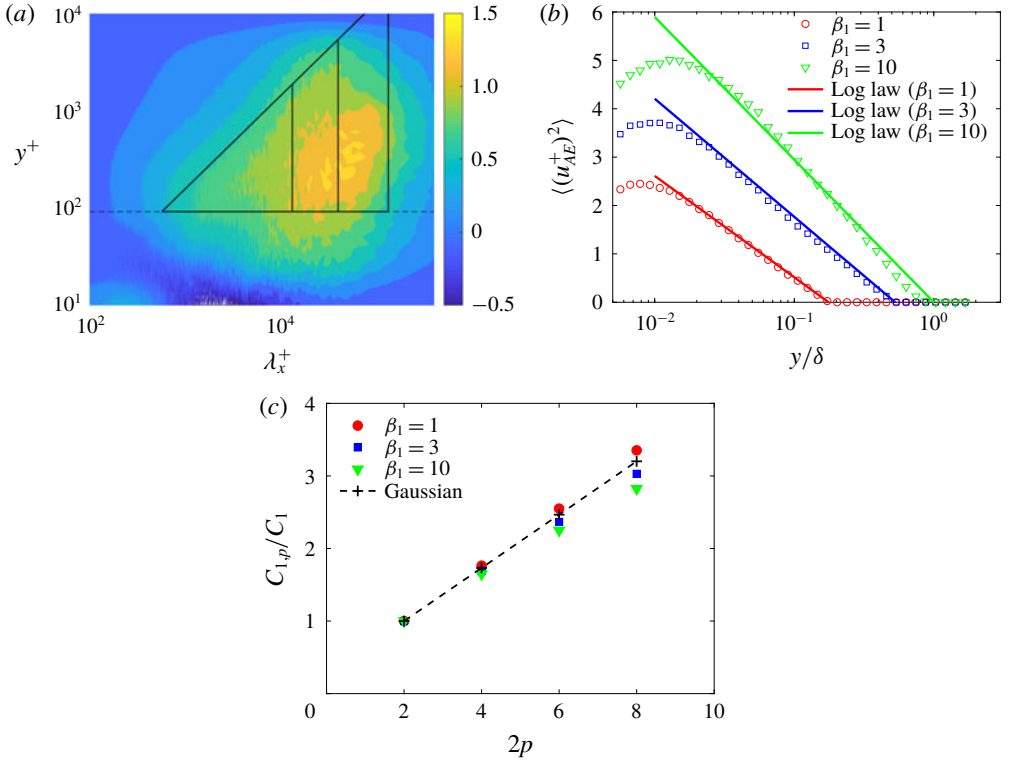


FIGURE 22. The effect of large-scale cutoff on the extracted statistics due to attached eddies. (*a*) The region due to attached eddies with different large-scale cutoff ($\beta_1 =$ 1, 3, 10). (*b*) The streamwise velocity variances due to attached eddies with different large-scale cutoffs as well as the predictions from the AEH, i.e. (3.2*a*.*b*). (*c*) The coefficient ratios $C_{1,p}/C_1$ of high-even-order moments as a function of moment order $2p$ for different large-scale cutoffs.

https://doi.org/10.1017/jfm.2019.980 Published online by Cambridge University Press

region is a trapezium for $\beta_1 = 10$ because it cuts off at $y = \delta$. As per our discussion in § 2.2, being conservative and using $\beta_1 = 1$, the extracted part of the flow will still be well modelled by the AEH; however, being very aggressive and using $\beta_1 = 10$, the statistical properties of the extracted part of the flow would not be captured by the AEH.

The streamwise velocity variances with different β_1 are shown in figure 22(*b*). The corresponding predictions from the AEH are given by solid lines, i.e. (3.2*a*,*b*). The large-scale cutoff shows up in δ_i hence the end location of the logarithmic scaling. The coefficient C_1 in (3.2*a*,*b*) increases as a function of the large-scale cutoff, the values of which are around 0.9, 1.0 and 1.3 for $\beta_1 = 1$, 3 and 10, respectively. The results for $\beta_1 = 1$ and 3 agree well with the AEH, whereas the result for $\beta_1 = 10$ deviates from the expected logarithmic scaling. Figure 22(*c*) shows the measured $C_{1,p}/C_1$ for high-even-order moments. The use of $\beta_1 = 1$ or $\beta_1 = 3\delta$ leads to Gaussian behaviour, which agrees well with the AEH, but $\beta_1 = 10$ results in sub-Gaussian behaviour, similar to the total velocity (Meneveau & Marusic 2013).

REFERENCES

ABE, H., KAWAMURA, H. & CHOI, H. 2004 Very large-scale structures and their effects on the wall shear-stress fluctuations in a turbulent channel flow up to $Re_\tau = 640$. *J. Fluids Engng* **126** (5), 835–843.

ADRIAN, R. J. 2007 Hairpin vortex organization in wall turbulence. *Phys. Fluids* **19** (4), 041301.

ADRIAN, R. J., MEINHART, C. D. & TOMKINS, C. D. 2000 Vortex organization in the outer region of the turbulent boundary layer. *J. Fluid Mech.* **422**, 1–54.

AGOSTINI, L. & LESCHZINER, M. 2017 Spectral analysis of near-wall turbulence in channel flow at $Re_\tau = 4200$ with emphasis on the attached-eddy hypothesis. *Phys. Rev. Fluids* **2** (1), 014603.

AGOSTINI, L. & LESCHZINER, M. A. 2014 On the influence of outer large-scale structures on near-wall turbulence in channel flow. *Phys. Fluids* **26** (7), 075107.

ANDERSON, W. 2016 Amplitude modulation of streamwise velocity fluctuations in the roughness sublayer: evidence from large-eddy simulations. *J. Fluid Mech.* **789**, 567–588.

BAARS, W. J., HUTCHINS, N. & MARUSIC, I. 2017*a* Reynolds number trend of hierarchies and scale interactions in turbulent boundary layers. *Phil. Trans. R. Soc. Lond.* A **375** (2089), 20160077.

BAARS, W. J., HUTCHINS, N. & MARUSIC, I. 2017*b* Self-similarity of wall-attached turbulence in boundary layers. *J. Fluid Mech.* **823**, R2.

BAARS, W. J. & MARUSIC, I. 2020*a* Data-driven decomposition of the streamwise turbulence kinetic energy in boundary layers. Part 1. Energy spectra. *J. Fluid Mech.* **882**, A25.

BAARS, W. J. & MARUSIC, I. 2020*b* Data-driven decomposition of the streamwise turbulence kinetic energy in boundary layers. Part 2. Integrated energy and A_1. *J. Fluid Mech.* **882**, A26.

BAARS, W. J., TALLURU, K. M., HUTCHINS, N. & MARUSIC, I. 2015 Wavelet analysis of wall turbulence to study large-scale modulation of small scales. *Exp. Fluids* **56** (10), 188.

BAIDYA, R. 2016 Multicomponent velocity measurements in turbulent boundary layers. PhD thesis, The University of Melbourne.

BAIDYA, R., PHILIP, J., HUTCHINS, N., MONTY, J. & MARUSIC, I. 2017 Distance-from-the-wall scaling of turbulent motions in wall-bounded flows. *Phys. Fluids* **29** (2), 020712.

BALAKUMAR, B. J. & ADRIAN, R. J. 2007 Large- and very-large-scale motions in channel and boundary-layer flows. *Phil. Trans. R. Soc. Lond.* A **365** (1852), 665–681.

BANDYOPADHYAY, P. R. & HUSSAIN, A. K. M. F. 1984 The coupling between scales in shear flows. *Phys. Fluids* **27** (9), 2221–2228.

BERNARDINI, M. & PIROZZOLI, S. 2011 Inner/outer layer interactions in turbulent boundary layers: a refined measure for the large-scale amplitude modulation mechanism. *Phys. Fluids* **23** (6), 061701.

BROWN, G. L. & THOMAS, A. S. W. 1977 Large structure in a turbulent boundary layer. *Phys. Fluids* **20** (10), S243–S252.

https://doi.org/10.1017/jfm.2019.980 Published online by Cambridge University Press

CANTWELL, B. J. 1981 Organized motion in turbulent flow. *Annu. Rev. Fluid Mech.* **13** (1), 457–515.

CHEN, X., HUSSAIN, F. & SHE, Z.-S. 2018 Quantifying wall turbulence via a symmetry approach. Part 2. Reynolds stresses. *J. Fluid Mech.* **850**, 401–438.

CHENG, C., LI, W., LOZANO-DURAN, A. & LIU, H. 2019 Identity of attached eddies in turbulent channel flows with bidimensional empirical mode decomposition. *J. Fluid Mech.* **870**, 1037–1071.

CHRISTENSEN, K. T. & ADRIAN, R. J. 2001 Statistical evidence of hairpin vortex packets in wall turbulence. *J. Fluid Mech.* **431**, 433–443.

CHUNG, D., MARUSIC, I., MONTY, J. P., VALLIKIVI, M. & SMITS, A. J. 2015 On the universality of inertial energy in the log layer of turbulent boundary layer and pipe flows. *Exp. Fluids* **56** (7), 141.

CHUNG, D. & MCKEON, B. J. 2010 Large-eddy simulation of large-scale structures in long channel flow. *J. Fluid Mech.* **661**, 341–364.

DAVIDSON, P. A., NICKELS, T. B. & KROGSTAD, P.-Å. 2006 The logarithmic structure function law in wall-layer turbulence. *J. Fluid Mech.* **550**, 51–60.

DE SILVA, C. M., HUTCHINS, N. & MARUSIC, I. 2016 Uniform momentum zones in turbulent boundary layers. *J. Fluid Mech.* **786**, 309–331.

DE SILVA, C. M., MARUSIC, I., WOODCOCK, J. D. & MENEVEAU, C. 2015 Scaling of second-and higher-order structure functions in turbulent boundary layers. *J. Fluid Mech.* **769**, 654–686.

DEL ÁLAMO, J. C., JIMÉNEZ, J., ZANDONADE, P. & MOSER, R. D. 2004 Scaling of the energy spectra of turbulent channels. *J. Fluid Mech.* **500**, 135–144.

DEL ÁLAMO, J. C., JIMÉNEZ, J., ZANDONADE, P. & MOSER, R. D. 2006 Self-similar vortex clusters in the turbulent logarithmic region. *J. Fluid Mech.* **561**, 329–358.

DENG, S., PAN, C., WANG, J. & HE, G. 2018 On the spatial organization of hairpin packets in a turbulent boundary layer at low-to-moderate Reynolds number. *J. Fluid Mech.* **844**, 635–668.

DOGAN, E., HANSON, R. E. & GANAPATHISUBRAMANI, B. 2016 Interactions of large-scale free-stream turbulence with turbulent boundary layers. *J. Fluid Mech.* **802**, 79–107.

DOGAN, E., ÖRLÜ, R., GATTI, D., VINUESA, R. & SCHLATTER, P. 2019 Quantification of amplitude modulation in wall-bounded turbulence. *Fluid Dyn. Res.* **51** (1), 011408.

DUVVURI, S. & MCKEON, B. J. 2015 Triadic scale interactions in a turbulent boundary layer. *J. Fluid Mech.* **767**, R4.

GANAPATHISUBRAMANI, B. 2018 Law of the wall for small-scale streamwise turbulence intensity in high-Reynolds-number turbulent boundary layers. *Phys. Rev. Fluids* **3** (10), 104607.

GANAPATHISUBRAMANI, B., HUTCHINS, N., MONTY, J. P., CHUNG, D. & MARUSIC, I. 2012 Amplitude and frequency modulation in wall turbulence. *J. Fluid Mech.* **712**, 61–91.

GANAPATHISUBRAMANI, B., LONGMIRE, E. K. & MARUSIC, I. 2003 Characteristics of vortex packets in turbulent boundary layers. *J. Fluid Mech.* **478**, 35–46.

GE, M.-W., YANG, X. I. A. & MARUSIC, I. 2019 Velocity probability distribution scaling in wall-bounded flows at high Reynolds numbers. *Phys. Rev. Fluids* **4**, 034101.

GRAHAM, J., KANOV, K., YANG, X. I. A., LEE, M., MALAYA, N., LALESCU, C. C., BURNS, R., EYINK, G., SZALAY, A., MOSER, R. D. *et al.* 2016 A web services accessible database of turbulent channel flow and its use for testing a new integral wall model for LES. *J. Turbul.* **17** (2), 181–215.

GUALA, M., HOMMEMA, S. E. & ADRIAN, R. J. 2006 Large-scale and very-large-scale motions in turbulent pipe flow. *J. Fluid Mech.* **554**, 521–542.

GUALA, M., METZGER, M. & MCKEON, B. J. 2011 Interactions within the turbulent boundary layer at high Reynolds number. *J. Fluid Mech.* **666**, 573–604.

HAMILTON, J. M., KIM, J. & WALEFFE, F. 1995 Regeneration mechanisms of near-wall turbulence structures. *J. Fluid Mech.* **287**, 317–348.

HEAD, M. R. & BANDYOPADHYAY, P. 1981 New aspects of turbulent boundary-layer structure. *J. Fluid Mech.* **107**, 297–338.

HELLSTRÖM, L. H. O., MARUSIC, I. & SMITS, A. J. 2016 Self-similarity of the large-scale motions in turbulent pipe flow. *J. Fluid Mech.* **792**, R1.

https://doi.org/10.1017/jfm.2019.980 Published online by Cambridge University Press

HOWLAND, M. F. & YANG, X. I. A. 2018 Dependence of small-scale energetics on large scales in turbulent flows. *J. Fluid Mech.* **852**, 641–662.

HU, R. & ZHENG, X. 2018 Energy contributions by inner and outer motions in turbulent channel flows. *Phys. Rev. Fluids* **3** (8), 084607.

HULTMARK, M., VALLIKIVI, M., BAILEY, S. C. C. & SMITS, A. J. 2012 Turbulent pipe flow at extreme Reynolds numbers. *Phys. Rev. Lett.* **108** (9), 094501.

HUTCHINS, N. & MARUSIC, I. 2007*a* Evidence of very long meandering features in the logarithmic region of turbulent boundary layers. *J. Fluid Mech.* **579**, 1–28.

HUTCHINS, N. & MARUSIC, I. 2007*b* Large-scale influences in near-wall turbulence. *Phil. Trans. R. Soc. Lond.* A **365** (1852), 647–664.

HUTCHINS, N., NICKELS, T. B., MARUSIC, I. & CHONG, M. S. 2009 Hot-wire spatial resolution issues in wall-bounded turbulence. *J. Fluid Mech.* **635**, 103–136.

HWANG, J. & SUNG, H. J. 2018 Wall-attached structures of velocity fluctuations in a turbulent boundary layer. *J. Fluid Mech.* **856**, 958–983.

HWANG, Y. 2015 Statistical structure of self-sustaining attached eddies in turbulent channel flow. *J. Fluid Mech.* **767**, 254–289.

JIMÉNEZ, J. 2012 Cascades in wall-bounded turbulence. *Annu. Rev. Fluid Mech.* **44**, 27–45.

JIMÉNEZ, J. 2018 Coherent structures in wall-bounded turbulence. *J. Fluid Mech.* **842**, P1.

JIMÉNEZ, J. & HOYAS, S. 2008 Turbulent fluctuations above the buffer layer of wall-bounded flows. *J. Fluid Mech.* **611**, 215–236.

JIMÉNEZ, J. & MOSER, R. D. 2007 What are we learning from simulating wall turbulence? *Phil. Trans. R. Soc. Lond.* A **365** (1852), 715–732.

JIMÉNEZ, J. & PINELLI, A. 1999 The autonomous cycle of near-wall turbulence. *J. Fluid Mech.* **389**, 335–359.

KATUL, G. & VIDAKOVIC, B. 1996 The partitioning of attached and detached eddy motion in the atmospheric surface layer using Lorentz wavelet filtering. *Boundary-Layer Meteorol.* **77** (2), 153–172.

KIM, K. C. & ADRIAN, R. J. 1999 Very large-scale motion in the outer layer. *Phys. Fluids* **11** (2), 417–422.

KOVASZNAY, L. S. G., KIBENS, V. & BLACKWELDER, R. F. 1970 Large-scale motion in the intermittent region of a turbulent boundary layer. *J. Fluid Mech.* **41** (2), 283–325.

LAVAL, J. P., VASSILICOS, J. C., FOUCAUT, J. M. & STANISLAS, M. 2017 Comparison of turbulence profiles in high-Reynolds-number turbulent boundary layers and validation of a predictive model. *J. Fluid Mech.* **814**, R2.

LEE, J. H. & SUNG, H. J. 2011 Very-large-scale motions in a turbulent boundary layer. *J. Fluid Mech.* **673**, 80–120.

LEE, M. K., MALAYA, N. & MOSER, R. D. 2013 Petascale direct numerical simulation of turbulent channel flow on up to 786k cores. In *2013 International Conference for High Performance Computing, Networking, Storage and Analysis*. IEEE Computer Society.

LEE, M. K. & MOSER, R. D. 2015 Direct numerical simulation of turbulent channel flow up to $Re_\tau \approx 5200$. *J. Fluid Mech.* **774**, 395–415.

LEE, M. K. & MOSER, R. D. 2019 Spectral analysis of the budget equation in turbulent channel flows at high Reynolds number. *J. Fluid Mech.* **860**, 886–938.

LIU, H., BO, T. & LIANG, Y. 2017 The variation of large-scale structure inclination angles in high Reynolds number atmospheric surface layers. *Phys. Fluids* **29** (3), 035104.

LIU, H., WANG, G. & ZHENG, X. 2019 Amplitude modulation between multi-scale turbulent motions in high-Reynolds-number atmospheric surface layers. *J. Fluid Mech.* **861**, 585–607.

LOZANO-DURÁN, A., FLORES, O. & JIMÉNEZ, J. 2012 The three-dimensional structure of momentum transfer in turbulent channels. *J. Fluid Mech.* **694**, 100–130.

MARUSIC, I., CHAUHAN, K. A., KULANDAIVELU, V. & HUTCHINS, N. 2015 Evolution of zero-pressure-gradient boundary layers from different tripping conditions. *J. Fluid Mech.* **783**, 379–411.

MARUSIC, I. & HEUER, W. D. C. 2007 Reynolds number invariance of the structure inclination angle in wall turbulence. *Phys. Rev. Lett.* **99** (11), 114504.

https://doi.org/10.1017/jfm.2019.980 Published online by Cambridge University Press

MARUSIC, I., MCKEON, B. J., MONKEWITZ, P. A., NAGIB, H. M., SMITS, A. J. & SREENIVASAN, K. R. 2010 Wall-bounded turbulent flows at high Reynolds numbers: recent advances and key issues. *Phys. Fluids* **22** (6), 065103.

MARUSIC, I. & MONTY, J. P. 2019 Attached eddy model of wall turbulence. *Annu. Rev. Fluid Mech.* **51**, 49–74.

MARUSIC, I., MONTY, J. P., HULTMARK, M. & SMITS, A. J. 2013 On the logarithmic region in wall turbulence. *J. Fluid Mech.* **716**, R3.

MATHIS, R., HUTCHINS, N. & MARUSIC, I. 2009 Large-scale amplitude modulation of the small-scale structures in turbulent boundary layers. *J. Fluid Mech.* **628**, 311–337.

MATHIS, R., HUTCHINS, N. & MARUSIC, I. 2011*a* A predictive inner-outer model for streamwise turbulence statistics in wall-bounded flows. *J. Fluid Mech.* **681**, 537–566.

MATHIS, R., MARUSIC, I., HUTCHINS, N. & SREENIVASAN, K. R. 2011*b* The relationship between the velocity skewness and the amplitude modulation of the small scale by the large scale in turbulent boundary layers. *Phys. Fluids* **23** (12), 121702.

MCKEON, B. J. & SHARMA, A. S. 2010 A critical-layer framework for turbulent pipe flow. *J. Fluid Mech.* **658**, 336–382.

MENEVEAU, C. & MARUSIC, I. 2013 Generalized logarithmic law for high-order moments in turbulent boundary layers. *J. Fluid Mech.* **719**, R1.

MONKEWITZ, P. A. & NAGIB, H. M. 2015 Large-Reynolds-number asymptotics of the streamwise normal stress in zero-pressure-gradient turbulent boundary layers. *J. Fluid Mech.* **783**, 474–503.

MONTY, J. P., HUTCHINS, N., NG, H. C. H., MARUSIC, I. & CHONG, M. S. 2009 A comparison of turbulent pipe, channel and boundary layer flows. *J. Fluid Mech.* **632**, 431–442.

MOURI, H. 2017 Two-point correlation in wall turbulence according to the attached-eddy hypothesis. *J. Fluid Mech.* **821**, 343–357.

MOURI, H., MORINAGA, T. & HAGINOYA, S. 2019 Unlikely existence of k_x^{-1} spectral law in wall turbulence: an observation of the atmospheric surface layer. *Phys. Fluids* **31** (3), 035103.

NICKELS, T. B., MARUSIC, I., HAFEZ, S. & CHONG, M. S. 2005 Evidence of the k_1^{-1} law in a high-Reynolds-number turbulent boundary layer. *Phys. Rev. Lett.* **95** (7), 074501.

PATHIKONDA, G. & CHRISTENSEN, K. T. 2017 Inner–outer interactions in a turbulent boundary layer overlying complex roughness. *Phys. Rev. Fluids* **2** (4), 044603.

PATHIKONDA, G. & CHRISTENSEN, K. T. 2019 Investigation of inner-outer interactions in a turbulent boundary layer using high-speed particle image velocimetry. *Phys. Rev. Fluids* **4** (3), 034607.

PERRY, A. E. & CHONG, M. S. 1982 On the mechanism of wall turbulence. *J. Fluid Mech.* **119**, 173–217.

PERRY, A. E., HENBEST, S. & CHONG, M. S. 1986 A theoretical and experimental study of wall turbulence. *J. Fluid Mech.* **165**, 163–199.

PERRY, A. E. & MARUSIC, I. 1995 A wall-wake model for the turbulence structure of boundary layers. Part 1. Extension of the attached eddy hypothesis. *J. Fluid Mech.* **298**, 361–388.

PHILIP, J., BAIDYA, R., HUTCHINS, N., MONTY, J. & MARUSIC, I. 2013 Spatial averaging of streamwise and spanwise velocity measurements in wall-bounded turbulence using v- and x-probes. *Meas. Sci. Technol.* **24**, 115302.

PULLIN, D. I., INOUE, M. & SAITO, N. 2013 On the asymptotic state of high Reynolds number, smooth-wall turbulent flows. *Phys. Fluids* **25** (1), 015116.

RAO, K. N., NARASIMHA, R. & NARAYANAN, M. A. B. 1971 The bursting phenomenon in a turbulent boundary layer. *J. Fluid Mech.* **48** (2), 339–352.

ROBINSON, S. K. 1991 Coherent motions in the turbulent boundary layer. *Annu. Rev. Fluid Mech.* **23**, 601–639.

SCHLATTER, P. & ÖRLÜ, R. 2010 Quantifying the interaction between large and small scales in wall-bounded turbulent flows: a note of caution. *Phys. Fluids* **22** (5), 051704.

SCHOPPA, W. & HUSSAIN, F. 2002 Coherent structure generation in near-wall turbulence. *J. Fluid Mech.* **453**, 57–108.

SHARMA, A. S. & MCKEON, B. J. 2013 On coherent structure in wall turbulence. *J. Fluid Mech.* **728**, 196–238.

https://doi.org/10.1017/jfm.2019.980 Published online by Cambridge University Press

SMITS, A. J., MCKEON, B. J. & MARUSIC, I. 2011 High-Reynolds number wall turbulence. *Annu. Rev. Fluid Mech.* **43**, 353–375.

TOMKINS, C. D. & ADRIAN, R. J. 2003 Spanwise structure and scale growth in turbulent boundary layers. *J. Fluid Mech.* **490**, 37–74.

TOWNSEND, A. 1976 *The Structure of Turbulent Shear Flow*. Cambridge University Press.

VALLIKIVI, M., HULTMARK, M. & SMITS, A. J. 2015 Turbulent boundary layer statistics at very high Reynolds number. *J. Fluid Mech.* **779**, 371–389.

VASSILICOS, J. C., LAVAL, J.-P., FOUCAUT, J.-M. & STANISLAS, M. 2015 The streamwise turbulence intensity in the intermediate layer of turbulent pipe flow. *J. Fluid Mech.* **774**, 324–341.

VINCENTI, P., KLEWICKI, J., MORRILL-WINTER, C., WHITE, C. M. & WOSNIK, M. 2013 Streamwise velocity statistics in turbulent boundary layers that spatially develop to high Reynolds number. *Exp. Fluids* **54** (12), 1629.

WALEFFE, F. 1997 On a self-sustaining process in shear flows. *Phys. Fluids* **9** (4), 883–900.

WANG, C., GAO, Q., WANG, J., WANG, B. & PAN, C. 2019 Experimental study on dominant vortex structures in near-wall region of turbulent boundary layer based on tomographic particle image velocimetry. *J. Fluid Mech.* **874**, 426–454.

WANG, G. & ZHENG, X. 2016 Very large scale motions in the atmospheric surface layer: a field investigation. *J. Fluid Mech.* **802**, 464–489.

WOODCOCK, J. D. & MARUSIC, I. 2015 The statistical behaviour of attached eddies. *Phys. Fluids* **27** (1), 015104.

YAMAMOTO, Y. & TSUJI, Y. 2018 Numerical evidence of logarithmic regions in channel flow at $Re_\tau = 8000$. *Phys. Rev. Fluids* **3** (1), 012602.

YANG, H. & BO, T. 2018 Scaling of wall-normal turbulence intensity and vertical eddy structures in the atmospheric surface layer. *Bound.-Layer Meteor.* **166**, 199–216.

YANG, X. I. A., BAIDYA, R., JOHNSON, P., MARUSIC, I. & MENEVEAU, C. 2017 Structure function tensor scaling in the logarithmic region derived from the attached eddy model of wall-bounded turbulent flows. *Phys. Rev. Fluids* **2** (6), 064602.

YANG, X. I. A., BAIDYA, R., LV, Y. & MARUSIC, I. 2018 Hierarchical random additive model for the spanwise and wall-normal velocities in wall-bounded flows at high Reynolds numbers. *Phys. Rev. Fluids* **3** (12), 124606.

YANG, X. I. A., MARUSIC, I. & MENEVEAU, C. 2016*a* Hierarchical random additive process and logarithmic scaling of generalized high order, two-point correlations in turbulent boundary layer flow. *Phys. Rev. Fluids* **1** (2), 024402.

YANG, X. I. A., MARUSIC, I. & MENEVEAU, C. 2016*b* Moment generating functions and scaling laws in the inertial layer of turbulent wall-bounded flows. *J. Fluid Mech.* **791**, R2.

YANG, X. I. A. & MENEVEAU, C. 2019 Hierarchical random additive model for wall-bounded flows at high Reynolds numbers. *Fluid Dyn. Res.* **51** (1), 011405.

https://doi.org/10.1017/jfm.2019.980 Published online by Cambridge University Press